



---

# EgoGroups: A Benchmark For Detecting Social Groups of People in the Wild

Jeffri Murrugarra-Llerena<sup>1</sup>, Pranav Chitale<sup>1</sup>, Zicheng Liu<sup>1</sup>, Kai Ao<sup>1</sup>, Yujin Ham<sup>2</sup>,  
Guha Balakrishnan<sup>2</sup>, Paola Cascante-Bonilla<sup>1</sup>

<sup>1</sup>Stony Brook University    <sup>2</sup>Rice University

[🌐 Project Page](#)    [📄 Repository](#)

## Abstract

Social group detection, or the identification of humans involved in reciprocal interpersonal interactions (e.g., family members, friends, and customers and merchants), is a crucial component of social intelligence needed for agents transacting in the world. The few existing benchmarks for social group detection are limited by low scene diversity and reliance on third-person camera sources (e.g., surveillance footage). Consequently, these benchmarks generally lack real-world evaluation on how groups form and evolve in diverse cultural contexts and unconstrained settings. To address this gap, **we introduce *EgoGroups***, a first-person view dataset that captures social dynamics in cities around the world. *EgoGroups* spans 65 countries covering low, medium, and high-crowd settings under four weather/time-of-day conditions. We include dense human annotations for person and social groups, along with rich geographic and scene metadata. Using this dataset, we performed an extensive evaluation of state-of-the-art VLM/LLMs and supervised models on their group detection capabilities. We found several interesting findings, including VLMs and LLMs can outperform supervised baselines in a zero-shot setting, while crowd density and cultural regions clearly influence model performance.

## 1. Introduction

Humans in public environments often interact and move in social groups. A social group consists of two or more persons reciprocally engaged in an interaction or activity, rather than simply being co-located in a space. Families shopping together, people conversing, and a customer and merchant exchanging goods are valid groupings, whereas strangers waiting at a bus stop, commuters walking in the same direction, and a concert crowd as a whole are not. Understanding group membership and actions is therefore fundamental to how we as humans navigate and interact with others in realistic environments. As research advances toward the deployment of embodied agents and other assistive devices in real-world settings, it is crucial for these technologies to reason about how humans approach, join, or avoid groups from a first-person perspective (e.g., from camera-mounted perspective), rather than from fixed, calibrated camera arrays. While research on first-person camera-view datasets has made significant progress with respect to social attention and conversational cues [23, 35], they do not directly evaluate group membership, continuity, or group-level activities.

A core challenge in social group understanding is the inherent complexity of first-person visual perception. First-person videos exhibit rapid viewpoint change, motion blur, and frequent occlusions. Fields-of-view are often narrow and, when coupled with abrupt entry and exit of people in the camera’s view, lead to dramatic variations in scale and focus based on proximity to the camera wearer.

---

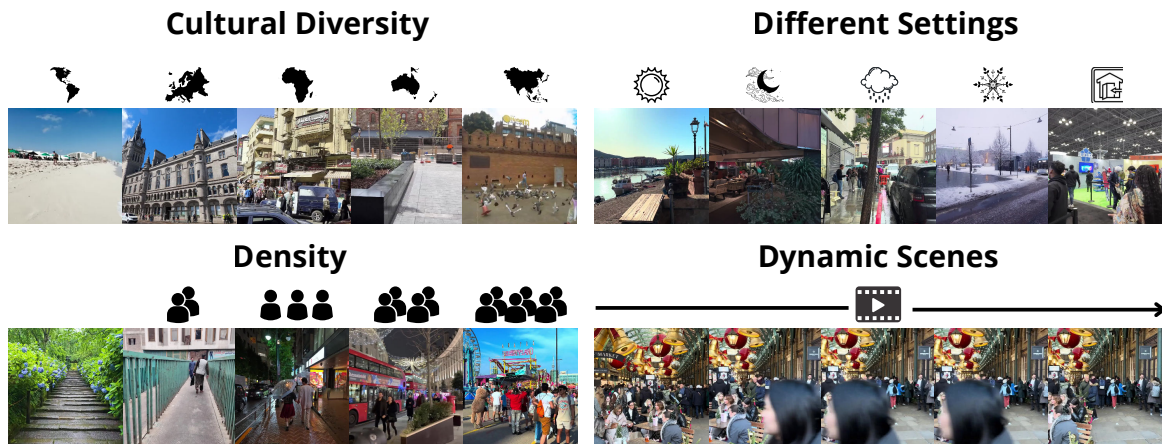


Figure 1 | *EgoGroups* is a dataset that captures social group behavior from walking-tour videos in cities around the world. We show culturally diverse settings with large groups of people or isolated pedestrians, in videos with a narrow, constantly moving field-of-view with frequent motion blur and occlusions.

These factors degrade the positional and orientational cues (proximity, head/body pose) that underlie group reasoning and make frame-level classification unreliable without robust tracking and temporal aggregation. Moreover, scene context strongly influences the likelihood of group memberships. In particular, location and crowd density impact visual statistics and spacing norms, causing a failure in generalization of model performance across locations. Additionally, cultural context amplifies these shifts; interpersonal spacing and orientation norms vary measurably across countries and regions, altering what constitutes “near,” “with” or “approaching” in public. Prior works report systematic differences in preferred distances between individuals and groups of people around the globe depending on country and region [2, 10, 21, 40].

While recent years have recorded significant progress towards social group detection, existing benchmarks [5, 58, 20, 32] primarily rely on third-person camera sources and are focused on specific scenarios. For instance, JRDB [20] annotates social groups observed from the perspective of a robot navigating a single location (Adelaide University campus), CAFE [32] captures interactions exclusively in 6 cafes with four static cameras, and PANDA [58] employs a static gigapixel camera in 21 distinct locations. Overall, these datasets are predominantly collected in a single city or country, reflecting a homogeneous demographic, consequently not accounting for the cultural variation in how social groups form and behave across different societies. Thus, our work is motivated by the lens of diversity and real-world representativeness.

This study introduces *EgoGroups*, a dataset and benchmark centered on first-person walking tour videos in diverse urban settings and crowd densities around the world, designed to evaluate group detection under real-world camera motions and settings. *EgoGroups* spans over 65 countries, totaling 540 video clips (roughly 45 minutes of total footage annotated from an initial raw video set of 16 hours) collected across a global range of cities and venue types. We took special care to select clips encompassing the full diversity of real-world scenarios, interactions, and group activities encountered in everyday life. For each video clip, we also provide fine-grained person detections, social group annotations, and geography/scene metadata (city, venue, density, and time-of-day), as illustrated in Figure 1 and 3. Captured scenes range from nearly empty sidewalks to highly congested markets and transit hubs, with some frames containing up to 26 annotated social groups. By combining first-person view videos with variation in crowd density in various locales, *EgoGroups* reveals a variety of group

configurations that are largely absent from existing first-person view and panoramic video benchmarks for group detection. Beyond group detection annotations, we also augment *EgoGroups* with computed statistics of crowd density, time-of-day, indoor/outdoor context, weather, and cultural regions, and used multiple VLM families to derive pseudo-labels for social activities and inter-person interactions (e.g., sightseeing, drinking, shopping, cooking, moving goods).

Using *EgoGroups*, we performed a thorough performance evaluation on a suite of state-of-the-art general-purpose VLMs and LLMs on the group detection task. We considered combinations of image, image-and-metadata, and metadata-only variants of these models, *without any task-specific fine-tuning*. The best performing models achieve 66.0 AP (Qwen2.5 VLM [7]) and 32.4 F1 score (Gemini 3-Pro). In addition, our results highlight that multiple factors annotated in our benchmark, such as crowd density and world region, significantly affect model performances. For example, models achieved particularly poor performance in underrepresented regions such as Africa and the Middle East, highlighting biases in their general learned representations with respect to specific appearance and action cues of the people and or environment of these regions. For example, our dataset statistics suggest that some actions, such as hand-holding, are far more prevalent in parts of Europe and North America than Africa, which could contribute to this performance discrepancy. Finally, we empirically confirmed that these foundation models without task-specific fine-tuning are still superior to fully supervised baselines on JRDB-Act [20] that rely on hand-crafted features such as spatial relationships, facial directions, trajectory patterns, and/or individually cropped person features. Hence, while VLM/LLM foundation models are now also the state-of-the-art on social group detection, they still exhibit a clear gap with respect to human perception that warrants further study and exploration.

In summary, this study makes the following contributions: (i) we introduce *EgoGroups*, a first-person view dataset of walking-tour videos from diverse cities that includes dense annotations for social groups and rich scene metadata, enabling realistic social group evaluation across regions, crowd density, and weather conditions; (ii) we probe a suite of state-of-the-art VLMs and LLMs on social group detection, demonstrating that they surpass fully supervised baselines on JRDB-Act without task-specific fine-tuning; (iii) we perform a quantitative analysis of crowds and social activities across regions, revealing density and culture-dependent patterns, and highlighting current limits in visual grounding and temporal aggregation for group perception in the wild.

## 2. Related Works

**Group Detection.** There are several studies on detecting groups from video recordings of moving people. Most cluster trajectories based on simple motion features [22, 30, 48, 61, 62]. Another line of work focuses on classifying conversational group structures [28, 55] by detecting pre-defined constructs, e.g., “f-formations” and “o-structures.” There are related studies on discovering social roles in groups from images/videos [46, 51], e.g., parent-child. All of these studies demonstrate their results on a few simple video sequences often shot from an overhead angle (without severe occlusions). In contrast, our goal is to learn subtle patterns from complex, first-person view data, without prior assumptions.

A few existing works focus on group future state prediction [3, 4, 13]. They use limited data (two pedestrian datasets), aerial views (avoiding occlusions), non-stochastic future prediction, and do not explicitly take neighboring effects and environment into account. Future prediction of people (not considering group structure) [1, 12, 25, 26, 36, 37] is a more well-studied research area. There are also several studies on detecting group activities [59, 62], and on surveillance and tracking of pedestrians [8, 9, 14, 57]. However, these works do not make predictions of future states.

Benchmarks in this line are often indoor with controlled recordings with synchronized sensors or outdoor with limited dynamics. For instance, SALSA [5] offers an indoor dataset containing group social annotations for only two scenarios (poster presentations and cocktail parties), captured using static overhead cameras that oversimplify real-world conditions. Other datasets, including SCU-VSD [53], GVEII [52], and PANDA [58], introduce outdoor scenes but use surveillance or fixed-mount cameras. Recent work introduced more dynamic environment: JLSG [19] annotates social groups in the CUB [17] dataset which has handheld cameras videos, and JRDB-Act [20] creates their own dataset by traversing indoor and outdoor spaces at Adelaide University with a robot-mounted panoramic camera and provide social grouping and activity labels. However, both remain limited on diverse scenarios and locations. MINGLE [38] offers broader diversity but depends solely on static images and quasi-stationary viewpoints sourced from Google Street View. In contrast, *EgoGroups* covers a large number of distinct locations and represents our human perspective, emulating day-to-day interactions that more effectively capture real-world dynamics and represent a harder challenge for current models.

A closely related line of work is modeling pedestrian movement. CityWalkers [39] is a large-scale dataset of YouTube-curated videos, which leverages pre-trained model-based labeling for individual and scene attributes. This work trains PedGen on CityWalkers to simulate the movement of individuals. Other works [6, 33, 24] predict pedestrian trajectories, accounting for human-human interactions, and demonstrating efficacy in crowded environments. Introvert [50] uses conditional visual attention to attend to relevant scene elements. However, these works focus on single pedestrian movements, and do not account for the context of human group activities or group detection.

**Cultural benchmarks.** As models become more capable, recent works have started looking at cultural benchmarks to tackle the Western-centric trends on LLMs and VLMs. CANDLE [44] extracts diverse cultural knowledge from a web corpus, including geography, religion, traditions, and preferences on food, drinks, and clothing. This knowledge serves as a foundation to assess LLMs’ cultural awareness. Following work [43, 16, 54], extend its application to VLMs introducing images, questions and answers with cultural context. Orthogonally, [34, 27] identify biases in models towards an ethnic group. ALM-Bench [56] and CVQA [47] incorporate different languages to further test cultural awareness in different contexts. Additional works test a complex cultural awareness by introducing visual grounding [49, 11] or text-to-images generation [29]. This trend highlights the importance and growing interest in evaluating the cultural robustness of large multimodal models; *EgoGroups* targets first-person view video and social-group structure, offering a complementary lens on how cultural context and crowd dynamics interact in real-world public environments.

### 3. *EgoGroups* Dataset

We overview *EgoGroups*, a dataset that captures social group behavior from walking-tour videos and aims to better represent social interactions across the globe. To establish a real-world evaluation setting for social group, we annotated our dataset with fine-grained detections and social grouping IDs. This section describes the data collection process (3.1), dataset statistics (3.2), the annotation procedures for coarse and fine-grained group detection (3.3–3.4), and the benchmark metrics (3.5).

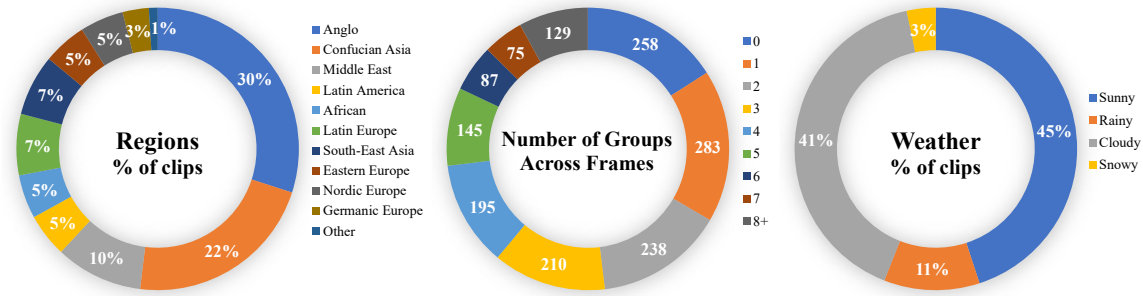


Figure 2 | Statistics of *EgoGroups*. Distribution of clips by region (left), number of annotated groups (middle) and by weather (right).

### 3.1. Data collection

Our dataset consists of a subset of videos from the Sekai dataset [35], and a complementary subset of walking-tour videos from YouTube that includes underrepresented cities (e.g., Kenya, Costa Rica, Nepal, etc), totaling over 16 hours. We use the official Sekai source code to download a portion of the Sekai-Real-HQ subset. For our complementary collection, we search and adapt the Sekai download procedure to avoid overlapping cities. We create 5-second clips by sampling from a video at 15-second intervals. We repeat this procedure until the end of each video. For our curated subset, we discard the first two-minute clips, as walking videos often feature highlight moments and frequent scene cuts in their opening segments. Following prior work [35], we use a VLM (i.e., Qwen2.5-VL 72B [7]) to perform data curation and cleaning, including discarding clips containing significant scene cuts; categorizing the crowd density, weather, time of day, and indoor/outdoor location. We also leverage country and city information from YouTube metadata. From this 16-hour pool, *EgoGroups* samples 540 clips (approximately 45 minutes), equally distributed across the three crowd density levels (scattered, moderate, and crowded), comprising 421 clips from the Sekai subset and 119 from our own subset.

### 3.2. Dataset Statistics

In total, *EgoGroups* contains clips from 65 countries and 128 cities. Our dataset includes metadata for different levels of crowd density (scattered, moderate, and crowded), time of day (day, night), weather conditions (sunny, cloudy, rainy, and snowy), and an additional distinction between indoor and outdoor environments (see Figure 2 (right) for a detailed percentage distribution of weather). *EgoGroups* contains 77.96% Sekai clips, while the remaining 22.03% consists of totally new clips from underrepresented cities. Figure 2 (left), shows the percentage of clips aggregated by region according to the Global Leadership and Organizational Behavior Effectiveness (GLOBE) [18, 42]. The category “Other” includes countries not covered by this survey, which are often underrepresented, such as Bermuda, Saint Lucia, and the Holy See. A fine-grained count is provided in the supplementary material.

### 3.3. Coarse Social Group Annotation

To obtain ground-truth labels for social groups, we manually annotate *EgoGroups*. We design a web-based interface for the annotation process, requiring annotators to draw bounding boxes and assign a confidence score on a Likert scale (1 to 5, where higher is more confident) to groups detected in a set of representative frames temporally distributed across each clip. Annotators also had the choice to view the full clip to resolve ambiguous cases. We organized the 540 clips into 36 tasks of 15 clips

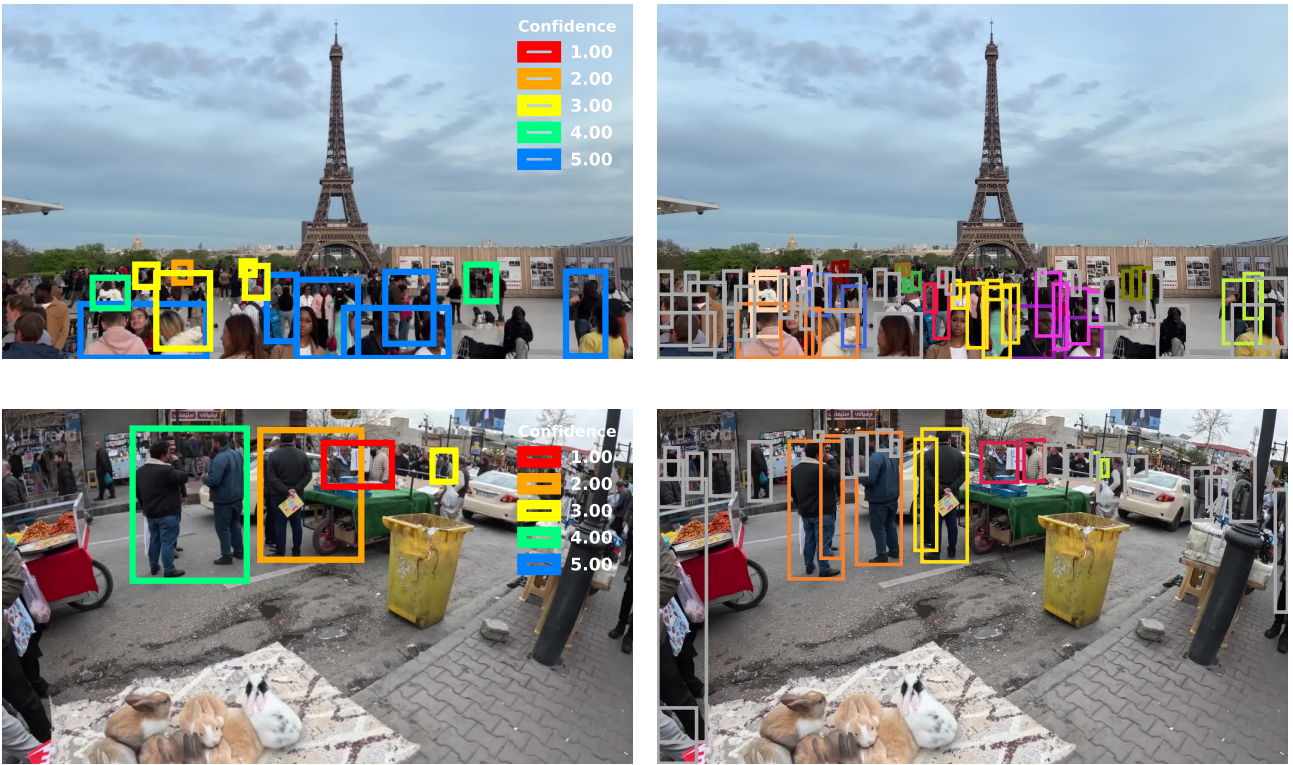


Figure 3 | **Annotation samples in *EgoGroups***. We show group detections with varying annotator confidence levels (red = lowest, blue = highest) and corresponding fine-grained annotations (individuals marked in gray).

each with a specific frame, and distributed the annotation tool. Each frame has at least 3 distinct annotators. Finally, to create a single annotation set, we iterate through each detected group and add it only if it does not overlap ( $\text{IoU} \geq 0.3$ ) with a previously added bounding box. We follow this approach to maximize group detections, as individual annotators often miss some groups. Figure 2 (middle) presents the aggregated number of groups annotated across frames for our coarse group evaluation task, with at least two groups for most of the images, and a few with more than 8 annotations. Figure 3 provides examples illustrating different confidence levels for this grouping task. In particular, there are some frames with up to 26 groups in a single frame.

### 3.4. Fine-grained Social Group Annotation

First, we generate pseudo fine-grained annotations using SAM3 [15] detections; a step-by-step guide is provided in the supplementary material. If the center point of a detection lies within a coarse patch, its label is assigned as the smallest enclosing coarse annotation. To further refine these detections, we deploy a web-based interface where annotators can reassign the label of a detection, remove a detection or an entire group, and add a bounding box. On average, each annotated frame is reviewed by approximately three annotators, with an inter-annotator agreement of 95.56% with the preceding coarse annotations. Finally, to consolidate the annotations, we apply a majority-vote scheme with a connected-components heuristic: each group label must appear in at least half of the annotators, and candidate boxes across annotators are matched with an area-adaptive IoU. Only connected components with at least two members are retained and merged to produce the final fine-grained detections, yielding a fine-grained inter-annotator agreement score of 91.64%. Totally, we have 24.331 annotated bounding boxes and 5.151 groups. Figure 3 provides examples of the fine-grained annotations along with their initial candidate coarse annotation.

### 3.5. Social Group Benchmark and Metrics

We use the JRDB-Act [20] dataset and *EgoGroups* as a benchmark for social group detection. Following prior works [60, 58, 20, 64], we use the annotated bounding boxes for evaluation and the following metrics. We evaluate social grouping with social average precision ( $G_1$ - $G_5$ , AP) metric used in JRDB-Act [20]. For each group, we establish correspondences between predicted and ground-truth groups by solving an optimal assignment problem, count true positives as matched boxes with  $\text{IoU} \geq 0.5$ , and compute average precision over all confidence thresholds. In addition, we evaluate the grouping IDs. Given the ground-truth ( $G_{\text{gt}}$ ) and predicted ( $G_{\text{det}}$ ) sets of persons, we consider  $G_{\text{det}}$  a true positive if  $\frac{|G_{\text{det}} \cap G_{\text{gt}}|}{\max(|G_{\text{det}}|, |G_{\text{gt}}|)} > 0.5$  and a false positive otherwise. Finally, we compute precision, recall, and F1.

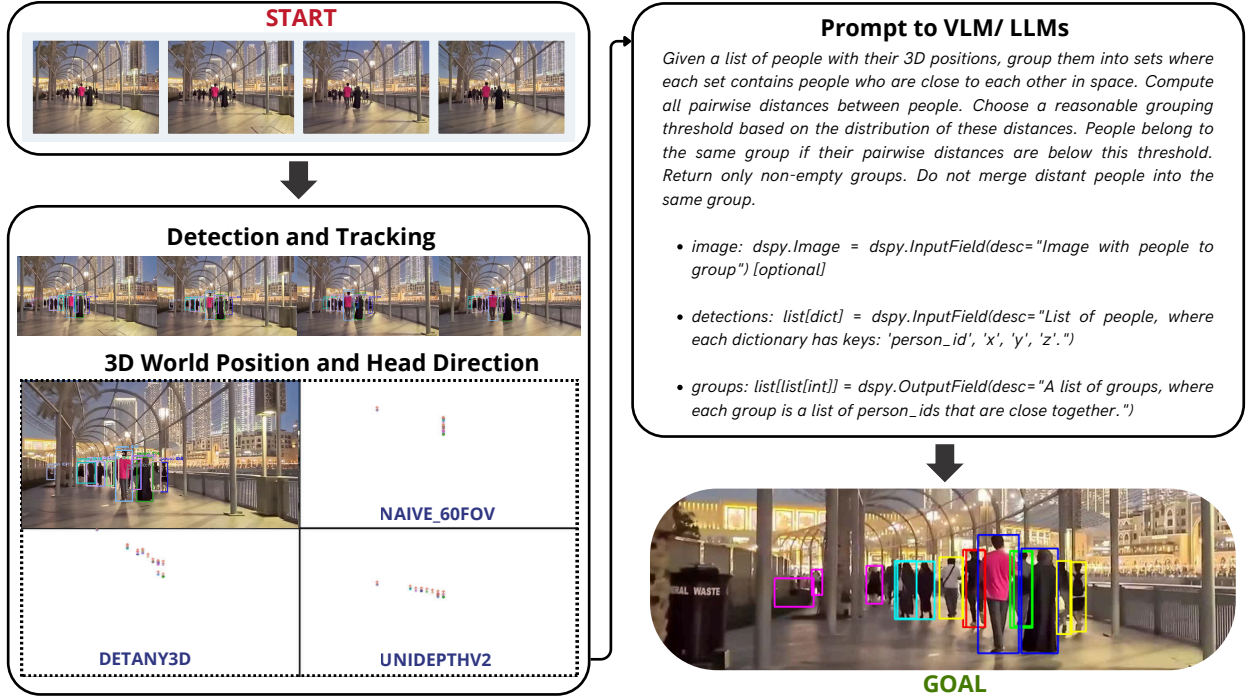


Figure 4 | **Overview of the pipeline for social grouping.** Our process involves bounding along with track\_ID to generate 3D metadata for an effective prompting.

## 4. Detecting Social Groups in the Wild

We implement a pipeline to obtain diverse metadata from bounding box within track ids (4.1) and develop an effective prompting strategy for LLMs and VLMs to detect groups in first-person view videos (4.2). The overall procedure is illustrated in Figure 4.

### 4.1. 3D metadata generation

Given a set of  $\mathbf{P}$  persons, where each  $\mathbf{p}_i$  consists of a track ID  $\mathbf{t}_i$  and a bounding box  $\mathbf{b}_i = (x_1, y_1, x_2, y_2)$  in the standard top-left and bottom-right format. For each person  $\mathbf{p}_i$ , we estimate their corresponding 3D world position to obtain depth-related information. This is a crucial and challenging step, as intrinsic and extrinsic camera parameters are often unavailable. We adopt two approaches:

- **Estimated intrinsics approach:** We assume an intrinsic camera ( $\mathbf{K}$ ) obtained from an estimated field of view (FOV). The optical center is obtained with  $c_x = W/2, c_y = H/2$ , where  $W$  and

H are the width and the height of the frame dimensions, respectively. Then, the focal length  $f_x = \frac{W/2}{\tan(\text{FOV}_x/2)}$ , where  $\text{FOV}_x$  is the field of view, we do similarly to obtain  $f_y$ . Finally, we compute 3D coordinate correspondences using classical 2D-to-3D projection formulas. For more details, ablation and full comparison with other approaches are presented in the supplementary material.

- **Off-the-shelf model approach:** We use pretrained models such as UniDepth-V2 [45] or DetAny3D [63]. Specifically, we provide each 2D bounding box to DetAny3D and query the center of the bbox to UniDepthV2 and retrieve the world coordinates from its prediction.

Finally, we aggregate  $\mathbf{w}_i = (x_i, y_i, z_i)$  for each person  $\mathbf{p}_i$ .

## 4.2. Prompt Design

We design specific prompt to query VLMs and LLMs. We use dspy [31] to standardize query generation and evaluation across different models, ensuring consistent comparisons. The model receives each person track\_ID with its corresponding 3D positions within a prompt to evoke group reasoning. For VLM, model receive the image alongside visual hints that link each track\_ID to the corresponding person. Prompt details are available in the appendix.

## 5. Experimental Results

Table 1 | Fine-grained performance comparison on *EgoGroups* dataset segmented by crowd density: scattered, moderate and crowded. Model combination indicates the backbone family, number of parameters, and modality.  $G_1$ – $G_5$  represent AP scores for group sizes 1–5+, with AP showing the average performance across all groups.

Model	Scattered							Moderate							Crowded							All
	G <sub>1</sub>	G <sub>2</sub>	G <sub>3</sub>	G <sub>4</sub>	G <sub>5</sub>	AP	G <sub>1</sub>	G <sub>2</sub>	G <sub>3</sub>	G <sub>4</sub>	G <sub>5</sub>	AP	G <sub>1</sub>	G <sub>2</sub>	G <sub>3</sub>	G <sub>4</sub>	G <sub>5</sub>	AP	AP			
Cosmos-Reason2	8B	VLM	57.18	74.42	76.36	75.35	80.6	72.78	28.92	45.28	59.54	68.02	68.55	54.06	12.8	30.12	50.05	61.53	73.18	45.53	51.07	
		LLM	60.72	71.03	72.84	70.49	75.0	70.02	32.47	49.61	65.81	62.54	76.02	57.29	20.58	40.56	55.9	59.69	65.15	48.38	53.38	
Qwen2.5	32B	VLM	58.94	83.37	<b>86.92</b>	<b>81.6</b>	<b>92.27</b>	<b>80.62</b>	30.28	62.72	77.55	<b>84.21</b>	79.38	66.83	19.11	52.42	73.26	76.05	71.56	58.48	63.37	
		LLM	63.71	85.28	82.38	79.51	62.73	74.72	40.49	73.14	75.28	73.02	70.62	66.51	30.45	64.66	72.69	68.27	64.38	60.09	63.54	
	72B	VLM	60.53	85.1	85.11	79.17	84.54	78.89	37.18	66.91	<b>79.14</b>	78.45	<b>82.76</b>	<b>68.89</b>	25.89	59.79	<b>73.79</b>	<b>77.81</b>	<b>74.18</b>	<b>62.29</b>	<b>66.00</b>	
		LLM	63.97	<b>85.84</b>	80.24	75.0	59.55	72.92	38.73	73.68	76.4	71.85	69.28	65.99	28.02	65.93	73.18	68.64	61.92	59.54	62.93	
Qwen3	30B	VLM	71.59	80.28	74.26	75.0	59.09	72.04	50.29	66.02	71.33	71.07	70.36	65.81	36.89	57.26	63.7	60.82	58.39	55.41	63.23	
		LLM	69.41	83.56	79.37	78.47	62.73	74.71	54.94	69.94	71.17	72.14	70.15	67.67	47.59	62.84	69.35	63.25	59.25	60.46	64.23	
Gemini-3-Pro		VLM	<b>82.67</b>	80.85	73.92	76.39	68.79	76.52	<b>70.37</b>	<b>75.5</b>	68.24	67.24	57.07	67.69	<b>63.09</b>	<b>69.78</b>	64.16	54.43	47.9	59.87	64.05	
		LLM	77.66	81.85	75.33	75.35	59.55	73.95	60.29	74.18	73.23	70.9	62.12	68.14	50.95	69.0	68.63	63.71	54.88	61.44	64.85	

**Detecting groups on *EgoGroups* benchmark** We conduct experiments across one proprietary and three open-source models: Qwen2.5, Qwen3, Cosmos-Reason2 and Gemini 3. We test both VLM and LLM counterparts for each model, covering 8B model for Cosmos-Reason2, 32B and 72B for Qwen2.5, 30B for Qwen3, as well as the Pro version for Gemini-3. VLM models receive an image and a prompt as input, whereas LLMs receive only a textual prompt. We evaluate VLM/LLMs using our fine-grained annotations and metrics across region and crowdness dimensions. The results are presented in Table 1, 2 and 3. In particular, Table 1 and 2 report the AP and F1 metric under varying crowd densities alongside with the overall performance. Table 3 shows AP results segmented by the GLOBE regions, highlighting the best (in red) and worst performance (in blue) row-wise.

Table 2 | Fine-grained performance comparison on *EgoGroups* dataset segmented by crowd density: scattered, moderate and crowded. Model combination indicates the backbone family, number of parameters, and modality. Precision, Recall, and F1 scores measure the false positive rate of predicted group IDs (without individuals).

Model			Scattered			Moderate			Crowded			All
			Precision	Recall	F1	Precision	Recall	F1	Precision	Recall	F1	F1
Cosmos-Reason2	8B	VLM	50.44	49.82	50.1	25.92	16.16	19.9	11.22	5.41	7.3	17.64
		LLM	44.73	40.6	42.47	22.04	14.3	17.33	11.75	6.61	8.45	15.93
Qwen2.5	32B	VLM	51.4	61.87	56.12	27.05	26.18	26.58	14.35	13.69	14.01	23.49
		LLM	51.22	64.05	56.88	29.8	33.25	31.41	17.5	21.74	19.38	27.70
	72B	VLM	52.77	<b>65.65</b>	58.49	32.76	33.54	33.1	21.0	22.25	21.6	29.97
		LLM	51.09	65.36	57.3	28.52	32.39	30.31	15.01	18.98	16.75	25.97
Qwen3	30B	VLM	54.88	56.73	55.7	30.02	25.69	27.68	13.73	12.45	13.06	23.11
		LLM	55.96	61.84	58.73	33.72	29.54	31.47	17.92	16.29	17.03	27.05
Gemini-3-Pro		VLM	<b>61.02</b>	57.83	<b>59.19</b>	<b>38.44</b>	<b>36.99</b>	<b>37.63</b>	<b>22.75</b>	<b>25.67</b>	<b>24.09</b>	<b>32.44</b>
		LLM	58.0	59.01	58.26	34.59	34.21	34.34	19.28	22.72	20.83	29.41

Table 3 | Fine-grained performance comparison on the *EgoGroups* dataset, segmented by GLOBE regions: African (AF), Anglo (AN), Confucian Asia (CA), Eastern Europe (EU), Germanic Europe (GE), Latin America (LA), Latin Europe (LE), Middle East (ME), Nordic Europe (NE), South-East Asia (SA), Other (O). Model combination indicates the backbone family, number of parameters, and input modality. We report each region’s AP score individually, and compute MAP as the average across all regions. The best and worst values per row are highlighted in red and blue, respectively.

Model			AF	AN	CA	EU	GE	LA	LE	ME	NE	SA	O
Cosmos-Reason2	8B	VLM	47.19	50.49	54.01	51.69	<b>40.07</b>	51.12	52.98	47.05	49.86	52.86	<b>58.89</b>
		LLM	<b>45.95</b>	<b>56.89</b>	55.25	54.59	50.95	54.17	54.40	49.18	51.21	52.95	53.37
Qwen2.5	32B	VLM	61.99	64.63	63.57	58.82	60.48	66.55	64.09	57.98	<b>71.75</b>	65.75	<b>50.00</b>
		LLM	61.87	65.01	62.16	61.69	62.84	<b>66.89</b>	63.84	<b>59.75</b>	69.36	63.28	61.63
	72B	VLM	<b>58.64</b>	67.24	65.78	64.54	67.06	<b>70.06</b>	67.69	59.42	71.45	67.30	65.80
		LLM	61.94	65.22	61.88	62.32	64.28	65.04	62.61	57.33	<b>67.31</b>	64.49	<b>54.21</b>
Qwen3	30B	VLM	56.07	64.76	58.49	60.26	<b>65.85</b>	59.92	63.42	<b>53.94</b>	56.30	64.20	63.10
		LLM	62.64	65.61	64.43	65.95	66.34	66.73	63.30	57.70	<b>67.66</b>	66.31	<b>55.60</b>
Gemini-3-Pro		VLM	62.41	66.70	64.01	68.23	65.53	64.79	64.32	<b>60.24</b>	<b>71.84</b>	66.03	62.31
		LLM	60.87	64.59	64.69	<b>68.61</b>	64.37	62.55	66.47	<b>59.51</b>	62.44	66.69	64.70

**Detecting Groups from Panoramic Views.** Table 4 shows experimental results on the JRDB-Act datasets. Performance is evaluated using fine grained Average Precision (AP), following the same setup as [20] across five group-size categories: single groups ( $G_1$ ), two groups ( $G_2$ ), three groups ( $G_3$ ), four groups ( $G_4$ ), and five or more groups ( $G_5$ ) as well the overall mean AP (AP). Along with these metrics, we present Precision, Recall and F1 score for groups excluding individuals. These results includes trained methods within this dataset.

**Detecting Social Activities on *EgoGroups*.** Moreover, we probe different VLM models to analyze activities and close interactions in the detected group. For each frame, we compute a bounding box for each group ( $B_{\text{group}}$ ) encompassing its members. We prompt different model versions of Qwen2.5-VL with the respective frame and  $B_{\text{group}}$  to describe activities in which members of a group are engaged, and answer whether or not there are close interactions within a group, particularly probing for hugging and hand-holding (results in the appendix). Activity descriptions are left open-ended, which leads

Table 4 | Fine-grained performance comparison on the JRDB dataset. Model combination indicates the backbone family, number of parameters, and input modality.  $G_1$ – $G_5$  represent AP scores for group sizes 1–5+, with AP showing the average performance across all groups. Precision, Recall, and F1 scores measure the false positive rate of predicted group IDs (without individuals).

Model			Group Detection (AP)					Group ID Prediction			
			G <sub>1</sub>	G <sub>2</sub>	G <sub>3</sub>	G <sub>4</sub>	G <sub>5</sub>	AP	Precision	Recall	F1
JLSG [19]			8.0	29.30	37.5	65.40	67.0	41.4	-	-	-
JRDB-Act [20]			81.40	64.80	49.10	63.20	37.20	59.2	-	-	-
DVT3 [60]			-	-	-	-	-	-	<b>61.16</b>	31.06	41.19
Cosmos-Reason2	8B	VLM	44.88	34.7	30.96	36.83	55.0	40.47	19.83	5.83	9.02
		LLM	48.47	36.19	29.05	31.71	56.26	40.34	24.7	6.93	10.82
Qwen2.5	32B	VLM	25.54	47.44	47.23	54.03	69.3	48.71	22.39	16.81	19.2
		LLM	35.13	56.78	54.11	56.96	69.49	54.49	28.45	23.88	25.97
	72B	VLM	28.4	45.44	43.62	51.26	71.99	48.14	23.54	17.28	19.93
		LLM	32.95	55.42	55.34	60.99	66.86	54.31	28.98	25.46	27.11
Qwen3	30B	VLM	30.5	44.2	41.5	44.71	72.48	46.68	30.19	17.45	22.12
		LLM	47.15	57.38	54.45	57.97	66.62	56.71	40.25	27.84	32.91
	235B	VLM	31.54	44.28	41.36	50.59	77.24	49.0	36.80	21.51	27.15
		LLM	31.0	51.29	60.4	69.63	<b>79.95</b>	58.46	34.03	25.53	29.17
Gemini-3-Pro	VLM	<b>56.66</b>	<b>71.79</b>	79.33	79.7	57.49	68.99	42.99	<b>46.38</b>	<b>44.62</b>	
	LLM	51.65	69.97	<b>82.52</b>	<b>81.8</b>	64.08	<b>70.0</b>	40.89	43.97	42.37	

to outcomes that are either verbs (e.g. *walking, socializing*) or longer descriptions such as *waiting to cross the street in snowy weather*. We prompt different VLM families (i.e., LLaVA-1.6, Qwen2.5-VL and DeepSeek-VL2) for this task. Figure 5 presents an example of activities across models. To enable further analysis with activity frequencies, we restrict the open-ended outputs to a fixed vocabulary by deduplicating semantically similar words and descriptions (e.g., *taking a stroll* and *walking in the city map* to *walk*). For this, we convert unique activity values to an embedding space using Qwen3-8B-Embedding and perform greedy matching based on cosine similarity. We then compute the frequencies of the activities in the vocabulary. Figure 6 shows count of clustered activities per region by Qwen2.5 VL 72B Instruct.

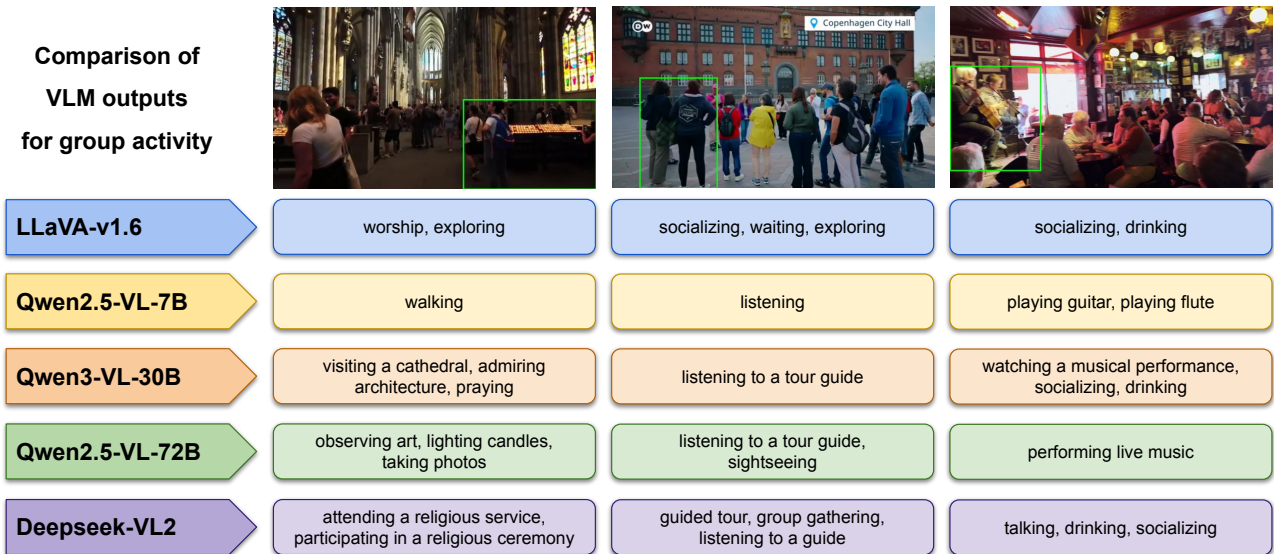


Figure 5 | Qualitative comparison of group activities predicted by VLMs for various scenarios.

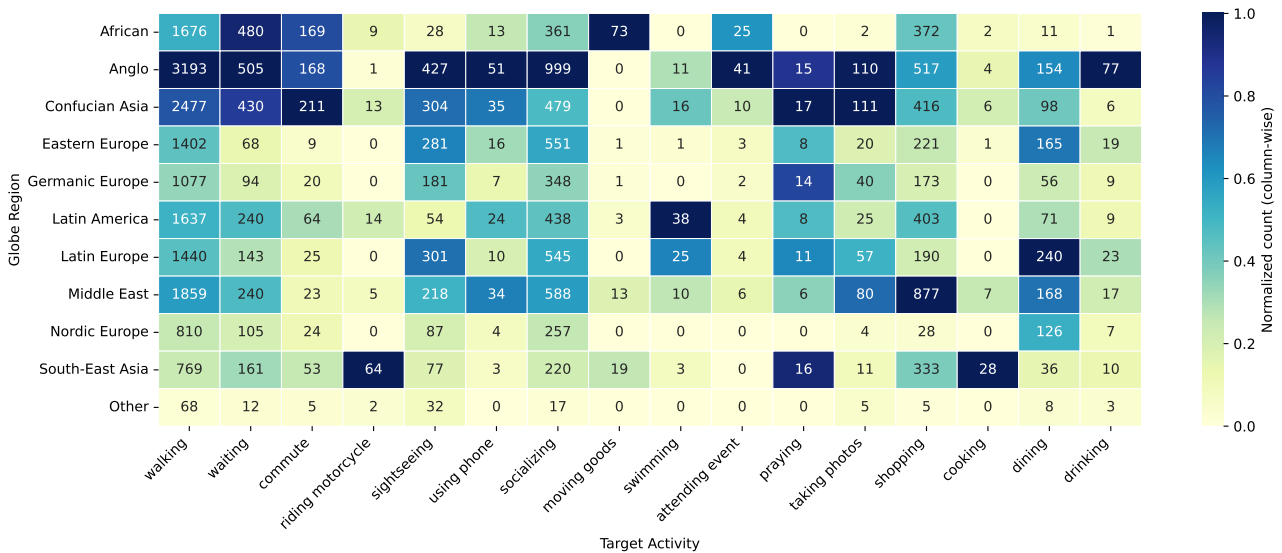


Figure 6 | Per-region activity count heatmap across GLOBE region by Qwen2.5-VL 72B Instruct. Column-wise color intensity reflects the relative frequency of each activity within each region.

## 6. Analysis

**Social Grouping.** On *EgoGroups*, we observe that larger models generally achieve higher AP, with Qwen 2.5 72B, 32B, and Gemini 3-Pro yielding the best performance. In particular, Qwen2.5VL 72B achieves 66.00 overall AP, while Gemini 3-Pro achieves 32.44 F1, outperforming all LLM variants of comparable size. When segmented by crowd density, the results reveal an expected pattern: as crowd density increases, the task becomes increasingly challenging for all models, yielding consistently lower scores in both metrics. For instance, best performance on scattered set drops from 80.62% to 62.29% in AP and from 59.19% to 32.44% in F1 score. Qualitative results in Figure 7 illustrate that VLM/LLMs can recover reasonable groupings in scattered and moderate scenes, but still struggle in the most crowded scenarios. Region-wise results reveal significant performance variation across GLOBE regions. Middle East (ME) and African (AF) regions consistently record the lowest scores, whereas Nordic Europe (NE), Anglo (AN), and Latin America (LA) prove less challenging for all models. Interestingly, the better-performing regions are largely or partially influenced by Western culture, suggesting that this disparity may reflect inherent biases in the models, where Western social contexts and interaction patterns are better represented.

On the JRDB-Act benchmark, smaller models tends to be better in groups  $G_1$  and  $G_2$ , and  $G_5$  are best in larger models. Gemini 3-Pro reaches 70.00 on AP and 44.62 on F1, outperforming the supervised baselines by +10.8 and +3.43 respectively. This suggests that current VLMs/LLMs can surpass trained models when perceptual metadata is available. However, some challenges remain; compared with DVT3 [60], VLMs and LLMs achieve better recall but lower precision, suggesting a tendency to over-predict group memberships, capturing more true groups at the cost of introducing false positives. In this dataset, LLMs consistently surpass VLMs of similar size when both are given access to structured metadata, which may be attributed to the panoramic image format.

**Activity Recognition.** Based on activity recognition results, we observe that certain actions exhibit a potential relation to a geographic context. For instance, “drinking” appears as a top activity in Latin Europe, Anglo, and the Middle East, while “moving goods” is prominent in Africa and “cooking” in South East Asia. Beyond the most frequent actions related to walking, waiting, and socializing, the



Figure 7 | Qualitative results of our approach across frames with varying crowd densities. From left to right: scattered, moderate, and crowded. Detections with the same color are judged to be in the same social group.

most frequent activities across models are: “moving goods” for Africa, “riding a motorcycle” for Asia. These patterns may reflect genuine behavioral differences captured in the first-person view videos; however, they could also reveal systematic biases in the training data or inherent cultural stereotypes encoded within the models. The prevalence of “moving goods” in Africa, for instance, may indicate the models’ tendency to associate this region with informal commerce, warranting careful examination of whether these predictions align with ground-truth annotations or represent model biases. To further validate this finding, we inspect different model outputs in the appendix.

## 7. Conclusion

In this work, we present *EgoGroups*, a dataset capturing social group behavior from first-person view walking-tour videos across diverse urban environments worldwide. We introduce a benchmark for social group detection that poses significant challenges to existing methods, enabling fine-grained performance analysis across crowd density levels and cultural regions, two aspects largely overlooked in prior work. To establish baseline performance, we leverage state-of-the-art VLMs and LLMs, outperforming existing baselines in both AP and F1 metrics, demonstrating the effectiveness of VLM/LLMs. Beyond performance, our analysis reveals meaningful cultural variations in activity patterns and social interactions across geographic regions, opening promising directions for studying cross-cultural embodied social behavior in vision and language models.

## Acknowledgments.

This material is based upon work supported by the SUNY AI Platform on Google Cloud (Phases 1&2).

## 8. Ethics Statement

**Data Collection and Privacy.** Our dataset consists of publicly available YouTube walking-tour videos. We do not attempt to identify individuals in the videos, and our annotations focus solely on group-level behaviors rather than individual identification. Furthermore, we make sure that all videos were filmed only in public spaces. *EgoGroups* is intended solely for the study of social groups and activity recognition within these social groups. We do not provide annotations for facial recognition or re-identification. We acknowledge that group detection could potentially be misused for surveillance or discriminatory purposes. We explicitly discourage the use of our dataset for such applications, and we emphasize *EgoGroups* for assistive technology and human-computer interaction rather than monitoring social groups in crowded spaces.

**Bias and Fairness.** Our analysis of cultural patterns in social behaviors is intended to uncover whether model predictions may reflect training data biases rather than genuine cultural patterns. The observed activity patterns across regions (Section 6) represent correlations in our specific dataset and should not be interpreted as definitive cultural characteristics.

**Annotations.** Our dataset labeling was conducted by university volunteers who were informed about the research purpose and were provided appropriate training.

## References

- [1] Afsar, P., Cortez, P., Santos, H.: Automatic human trajectory destination prediction from video. *Expert Systems with Applications* **110**, 41–51 (2018)
- [2] Aiello, J.R., Thompson, D.E.: Personal space, crowding, and spatial behavior in a cultural context. In: *Environment and culture*, pp. 107–178. Springer (1980)
- [3] Alahi, A., Goel, K., Ramanathan, V., Robicquet, A., Fei-Fei, L., Savarese, S.: Social lstm: Human trajectory prediction in crowded spaces. In: *Proceedings of the IEEE conference on computer vision and pattern recognition*. pp. 961–971 (2016)
- [4] Alahi, A., Ramanathan, V., Fei-Fei, L.: Socially-aware large-scale crowd forecasting. In: *Proceedings of the IEEE Conference on Computer Vision and Pattern Recognition*. pp. 2203–2210 (2014)
- [5] Alameda-Pineda, X., Staiano, J., Subramanian, R., Batrinca, L., Ricci, E., Lepri, B., Lanz, O., Sebe, N.: SALSA: A Novel Dataset for Multimodal Group Behavior Analysis. *IEEE Transactions on Pattern Analysis & Machine Intelligence* **38**(08), 1707–1720 (Aug 2016). doi:[10.1109/TPAMI.2015.2496269](https://doi.org/10.1109/TPAMI.2015.2496269), <https://doi.ieeecomputersociety.org/10.1109/TPAMI.2015.2496269>
- [6] Bae, I., Park, J.H., Jeon, H.G.: Learning pedestrian group representations for multi-modal trajectory prediction. In: *Proceedings of the European Conference on Computer Vision* (2022)
- [7] Bai, S., Chen, K., Liu, X., Wang, J., Ge, W., Song, S., Dang, K., Wang, P., Wang, S., Tang, J., et al.: Qwen2. 5-vl technical report. arXiv preprint arXiv:2502.13923 (2025)
- [8] Bazzani, L., Cristani, M., Murino, V.: Decentralized particle filter for joint individual-group tracking. In: *2012 IEEE Conference on Computer Vision and Pattern Recognition*. pp. 1886–1893. IEEE (2012)

- [9] Bazzani, L., Zanotto, M., Cristani, M., Murino, V.: Joint individual-group modeling for tracking. *IEEE transactions on pattern analysis and machine intelligence* **37**(4), 746–759 (2014)
- [10] Beaulieu, C.: Intercultural study of personal space: A case study. *Journal of applied social psychology* **34**(4), 794–805 (2004)
- [11] Bhatia, M., Ravi, S., Chinchure, A., Hwang, E., Shwartz, V.: From local concepts to universals: Evaluating the multicultural understanding of vision-language models. In: Al-Onaizan, Y., Bansal, M., Chen, Y.N. (eds.) *Proceedings of the 2024 Conference on Empirical Methods in Natural Language Processing*. pp. 6763–6782. Association for Computational Linguistics, Miami, Florida, USA (Nov 2024). doi:[10.18653/v1/2024.emnlp-main.385](https://doi.org/10.18653/v1/2024.emnlp-main.385), <https://aclanthology.org/2024.emnlp-main.385/>
- [12] Bi, H., Zhang, R., Mao, T., Deng, Z., Wang, Z.: How can i see my future? fvtraj: Using first-person view for pedestrian trajectory prediction. In: *Computer Vision–ECCV 2020: 16th European Conference, Glasgow, UK, August 23–28, 2020, Proceedings, Part VII 16*. pp. 576–593. Springer (2020)
- [13] Bisagno, N., Zhang, B., Conci, N.: Group lstm: Group trajectory prediction in crowded scenarios. In: *Proceedings of the European conference on computer vision (ECCV) workshops*. pp. 0–0 (2018)
- [14] Brunetti, A., Buongiorno, D., Trotta, G.F., Bevilacqua, V.: Computer vision and deep learning techniques for pedestrian detection and tracking: A survey. *Neurocomputing* **300**, 17–33 (2018)
- [15] Carion, N., Gustafson, L., Hu, Y.T., Debnath, S., Hu, R., Suris, D., Ryali, C., Alwala, K.V., Khedr, H., Huang, A., Lei, J., Ma, T., Guo, B., Kalla, A., Marks, M., Greer, J., Wang, M., Sun, P., Rädle, R., Afouras, T., Mavroudi, E., Xu, K., Wu, T.H., Zhou, Y., Momeni, L., Hazra, R., Ding, S., Vaze, S., Porcher, F., Li, F., Li, S., Kamath, A., Cheng, H.K., Dollár, P., Ravi, N., Saenko, K., Zhang, P., Feichtenhofer, C.: Sam 3: Segment anything with concepts (2025), <https://arxiv.org/abs/2511.16719>
- [16] Chiu, Y.Y., Jiang, L., Lin, B.Y., Park, C.Y., Li, S.S., Ravi, S., Bhatia, M., Antoniak, M., Tsvetkov, Y., Shwartz, V., Choi, Y.: CulturalBench: A robust, diverse and challenging benchmark for measuring LMs’ cultural knowledge through human-AI red-teaming. In: Che, W., Nabende, J., Shutova, E., Pilehvar, M.T. (eds.) *Proceedings of the 63rd Annual Meeting of the Association for Computational Linguistics (Volume 1: Long Papers)*. pp. 25663–25701. Association for Computational Linguistics, Vienna, Austria (Jul 2025). doi:[10.18653/v1/2025.acl-long.1247](https://doi.org/10.18653/v1/2025.acl-long.1247), <https://aclanthology.org/2025.acl-long.1247/>
- [17] Choi, W., Shahid, K., Savarese, S.: What are they doing? : Collective activity classification using spatio-temporal relationship among people. In: *2009 IEEE 12th International Conference on Computer Vision Workshops, ICCV Workshops*. pp. 1282–1289 (2009). doi:[10.1109/ICCVW.2009.5457461](https://doi.org/10.1109/ICCVW.2009.5457461)
- [18] Dorfman, P., Javidan, M., Hanges, P., Dastmalchian, A., House, R.: Globe: A twenty year journey into the intriguing world of culture and leadership. *Journal of World Business* **47**(4), 504–518 (2012). doi:<https://doi.org/10.1016/j.jwb.2012.01.004>, <https://www.sciencedirect.com/science/article/pii/S1090951612000053>, SPECIAL ISSUE: LEADERSHIP IN A GLOBAL CONTEXT

- [19] Ehsanpour, M., Abedin, A., Saleh, F., Shi, J., Reid, I., Rezatofghi, H.: Joint learning of social groups, individuals action and sub-group activities in videos. In: *Computer Vision – ECCV 2020: 16th European Conference, Glasgow, UK, August 23–28, 2020, Proceedings, Part IX*. p. 177–195. Springer-Verlag, Berlin, Heidelberg (2020). doi:[10.1007/978-3-030-58545-7\\_11](https://doi.org/10.1007/978-3-030-58545-7_11), [https://doi.org/10.1007/978-3-030-58545-7\\_11](https://doi.org/10.1007/978-3-030-58545-7_11)
- [20] Ehsanpour, M., Saleh, F., Savarese, S., Reid, I., Rezatofghi, H.: Jrdb-act: A large-scale dataset for spatio-temporal action, social group and activity detection. In: *Proceedings of the IEEE/CVF Conference on Computer Vision and Pattern Recognition* (2022)
- [21] Evans, G.W., Howard, R.B.: Personal space. *Psychological bulletin* **80**(4), 334 (1973)
- [22] Ge, W., Collins, R.T., Ruback, B.: Automatically detecting the small group structure of a crowd. In: *2009 workshop on applications of computer vision (WACV)*. pp. 1–8. IEEE (2009)
- [23] Grauman, K., Westbury, A., Byrne, E., Chavis, Z., Furnari, A., Girdhar, R., Hamburger, J., Jiang, H., Liu, M., Liu, X., Martin, M., Nagarajan, T., Radosavovic, I., Ramakrishnan, S.K., Ryan, F., Sharma, J., Wray, M., Xu, M., Xu, E.Z., Zhao, C., Bansal, S., Batra, D., Cartillier, V., Crane, S., Do, T., Doulaty, M., Erapalli, A., Feichtenhofer, C., Fragomeni, A., Fu, Q., Gebreselasie, A., González, C., Hillis, J., Huang, X., Huang, Y., Jia, W., Khoo, W., Kolář, J., Kottur, S., Kumar, A., Landini, F., Li, C., Li, Y., Li, Z., Mangalam, K., Modhugu, R., Munro, J., Murrell, T., Nishiyasu, T., Price, W., Puentes, P.R., Ramazanova, M., Sari, L., Somasundaram, K., Southerland, A., Sugano, Y., Tao, R., Vo, M., Wang, Y., Wu, X., Yagi, T., Zhao, Z., Zhu, Y., Arbeláez, P., Crandall, D., Damen, D., Farinella, G.M., Fuegen, C., Ghanem, B., Ithapu, V.K., Jawahar, C.V., Joo, H., Kitani, K., Li, H., Newcombe, R., Oliva, A., Park, H.S., Rehg, J.M., Sato, Y., Shi, J., Shou, M.Z., Torralba, A., Torresani, L., Yan, M., Malik, J.: Ego4d: Around the world in 3,000 hours of egocentric video. In: *2022 IEEE/CVF Conference on Computer Vision and Pattern Recognition (CVPR)*. pp. 18973–18990 (2022). doi:[10.1109/CVPR52688.2022.01842](https://doi.org/10.1109/CVPR52688.2022.01842)
- [24] Gupta, A., Johnson, J., Fei-Fei, L., Savarese, S., Alahi, A.: Social gan: Socially acceptable trajectories with generative adversarial networks. In: *IEEE Conference on Computer Vision and Pattern Recognition (CVPR)*. No. CONF (2018)
- [25] Hassan, M.A., Khan, M.U.G., Iqbal, R., Riaz, O., Bashir, A.K., Tariq, U.: Predicting humans future motion trajectories in video streams using generative adversarial network. *Multimedia Tools and Applications* **83**(5), 15289–15311 (2024)
- [26] Hu, A., Cotter, F., Mohan, N., Gurau, C., Kendall, A.: Probabilistic future prediction for video scene understanding. In: *Computer Vision–ECCV 2020: 16th European Conference, Glasgow, UK, August 23–28, 2020, Proceedings, Part XVI* 16. pp. 767–785. Springer (2020)
- [27] Huang, J.t., Qin, J., Zhang, J., Yuan, Y., Wang, W., Zhao, J.: VisBias: Measuring explicit and implicit social biases in vision language models. In: Christodoulopoulos, C., Chakraborty, T., Rose, C., Peng, V. (eds.) *Proceedings of the 2025 Conference on Empirical Methods in Natural Language Processing*. pp. 17981–18004. Association for Computational Linguistics, Suzhou, China (Nov 2025). doi:[10.18653/v1/2025.emnlp-main.908](https://doi.org/10.18653/v1/2025.emnlp-main.908), <https://aclanthology.org/2025.emnlp-main.908/>
- [28] Inaba, S., Aoki, Y.: Conversational group detection based on social context using graph clustering algorithm. In: *2016 12th International Conference on Signal-Image Technology & Internet-Based Systems (SITIS)*. pp. 526–531. IEEE (2016)

- [29] Jeong, S., Choi, I., Yun, Y., Kim, J.: Culture-TRIP: Culturally-aware text-to-image generation with iterative prompt refinement. In: Chiruzzo, L., Ritter, A., Wang, L. (eds.) Proceedings of the 2025 Conference of the Nations of the Americas Chapter of the Association for Computational Linguistics: Human Language Technologies (Volume 1: Long Papers). pp. 9543–9573. Association for Computational Linguistics, Albuquerque, New Mexico (Apr 2025). doi:[10.18653/v1/2025.naacl-long.483](https://doi.org/10.18653/v1/2025.naacl-long.483), <https://aclanthology.org/2025.naacl-long.483/>
- [30] Khan, S.D., Vizzari, G., Bandini, S., Basalamah, S.: Detection of social groups in pedestrian crowds using computer vision. In: Advanced Concepts for Intelligent Vision Systems: 16th International Conference, ACIVS 2015, Catania, Italy, October 26-29, 2015. Proceedings 16. pp. 249–260. Springer (2015)
- [31] Khattab, O., Singhvi, A., Maheshwari, P., Zhang, Z., Santhanam, K., Vardhamanan, S., Haq, S., Sharma, A., Joshi, T.T., Moazam, H., Miller, H., Zaharia, M., Potts, C.: Dspy: Compiling declarative language model calls into self-improving pipelines (2024)
- [32] Kim, D., Song, Y., Cho, M., Kwak, S.: Towards more practical group activity detection: A new benchmark and model. In: European Conference on Computer Vision (ECCV). pp. 240–258. Springer (2024)
- [33] Kothari, P., Kreiss, S., Alahi, A.: Human trajectory forecasting in crowds: A deep learning perspective. *Trans. Intell. Transport. Sys.* **23**(7), 7386–7400 (Jul 2022). doi:[10.1109/TITS.2021.3069362](https://doi.org/10.1109/TITS.2021.3069362), <https://doi.org/10.1109/TITS.2021.3069362>
- [34] Lee, T., Tu, H., Wong, C.H., Zheng, W., Zhou, Y., Mai, Y., Roberts, J.S., Yasunaga, M., Yao, H., Xie, C., Liang, P.: Vhelm: a holistic evaluation of vision language models. In: Proceedings of the 38th International Conference on Neural Information Processing Systems. NIPS '24, Curran Associates Inc., Red Hook, NY, USA (2024)
- [35] Li, Z., Li, C., Mao, X., Lin, S., Li, M., Zhao, S., Xu, Z., Li, X., Feng, Y., Sun, J., Li, Z., Zhang, F., Ai, J., Wang, Z., Wu, Y., He, T., Pang, J., Qiao, Y., Jia, Y., Zhang, K.: Sekai: A video dataset towards world exploration. arXiv preprint arXiv:2506.15675 (2025)
- [36] Liang, J., Jiang, L., Murphy, K., Yu, T., Hauptmann, A.: The garden of forking paths: Towards multi-future trajectory prediction. In: Proceedings of the IEEE/CVF Conference on Computer Vision and Pattern Recognition. pp. 10508–10518 (2020)
- [37] Liang, J., Jiang, L., Niebles, J.C., Hauptmann, A.G., Fei-Fei, L.: Peeking into the future: Predicting future person activities and locations in videos. In: Proceedings of the IEEE/CVF conference on computer vision and pattern recognition. pp. 5725–5734 (2019)
- [38] Liu, L., Kudaeva, A., Cipriano, M., Ghannam, F.A., Tan, F., de Melo, G., Sevtsuk, A.: Mingle: Vlms for semantically complex region detection in urban scenes (2025), <https://arxiv.org/abs/2509.13484>
- [39] Liu, Z., Lin, J., Wu, W., Zhou, B.: Learning to generate diverse pedestrian movements from web videos with noisy labels. In: The Thirteenth International Conference on Learning Representations (2025)
- [40] Lomranz, J.: Cultural variations in personal space. *The Journal of Social Psychology* **99**(1), 21–27 (1976)

- [41] McInnes, L., Healy, J., Melville, J.: Umap: Uniform manifold approximation and projection for dimension reduction (2020), <https://arxiv.org/abs/1802.03426>
- [42] Mensah, Y.M., Chen, H.: Global clustering of countries by culture – an extension of the globe study. SSRN Electronic Journal (Apr 2013). doi:10.2139/ssrn.2189904, available at SSRN: <https://ssrn.com/abstract=2189904> or <http://dx.doi.org/10.2139/ssrn.2189904>
- [43] Nayak, S., Jain, K., Awal, R., Reddy, S., Steenkiste, S.V., Hendricks, L.A., Stanczak, K., Agrawal, A.: Benchmarking vision language models for cultural understanding. In: Al-Onaizan, Y., Bansal, M., Chen, Y.N. (eds.) Proceedings of the 2024 Conference on Empirical Methods in Natural Language Processing. pp. 5769–5790. Association for Computational Linguistics, Miami, Florida, USA (Nov 2024). doi:10.18653/v1/2024.emnlp-main.329, <https://aclanthology.org/2024.emnlp-main.329/>
- [44] Nguyen, T.P., Razniewski, S., Varde, A., Weikum, G.: Extracting cultural commonsense knowledge at scale. In: Proceedings of the ACM Web Conference 2023. p. 1907–1917. WWW '23, Association for Computing Machinery, New York, NY, USA (2023). doi:10.1145/3543507.3583535, <https://doi.org/10.1145/3543507.3583535>
- [45] Piccinelli, L., Sakaridis, C., Yang, Y.H., Segu, M., Li, S., Abbeloos, W., Gool, L.V.: UniDepthV2: Universal monocular metric depth estimation made simpler (2025), <https://arxiv.org/abs/2502.20110>
- [46] Ramanathan, V., Yao, B., Fei-Fei, L.: Social role discovery in human events. In: Proceedings of the IEEE conference on computer vision and pattern recognition. pp. 2475–2482 (2013)
- [47] Romero, D., Lyu, C., Wibowo, H.A., Lynn, T., Hamed, I., Kishore, A.N., Mandal, A., Dragonetti, A., Abzaliev, A., Tonja, A.L., Balcha, B.F., Whitehouse, C., Salamea, C., Velasco, D.J., Adelani, D.I., Le Meur, D., Villa-Cueva, E., Koto, F., Farooqui, F., Belcavello, F., Batnasan, G., Vallejo, G., Caulfield, G., Ivetta, G., Song, H., Ademtew, H.B., Maina, H., Lovenia, H., Azime, I.A., Cruz, J.C.B., Gala, J., Geng, J., Ortiz-Barajas, J.G., Baek, J., Dunstan, J., Alemany, L.A., Nagasinghe, K.R.Y., Benotti, L., D’Haro, L.F., Viridiano, M., Estecha-Garitagoitia, M., Cabrera, M.C.B., Rodríguez-Cantelar, M., Jouitteau, M., Mihaylov, M., Etori, N., Imam, M.F.M., Adilazuarda, M.F., Gochoo, M., Otgonbold, M.E., Niyomugisha, O., Silva, P.M., Chitale, P., Dabre, R., Chevi, R., Zhang, R., Diandaru, R., Cahyawijaya, S., Góngora, S., Jeong, S., Purkayastha, S., Kuribayashi, T., Clifford, T., Jayakumar, T., Torrent, T.T., Ehsan, T., Araujo, V., Kementchedjhieva, Y., Burzo, Z., Lim, Z.W., Yong, Z.X., Ignat, O., Nwatu, J., Mihalcea, R., Solorio, T., Aji, A.F.: Cvqa: culturally-diverse multilingual visual question answering benchmark. In: Proceedings of the 38th International Conference on Neural Information Processing Systems. NIPS '24, Curran Associates Inc., Red Hook, NY, USA (2024)
- [48] Sandıkçı, S., Zinger, S., de With, P.H.: Detection of human groups in videos. In: Advanced Concepts for Intelligent Vision Systems: 13th International Conference, ACIVS 2011, Ghent, Belgium, August 22-25, 2011. Proceedings 13. pp. 507–518. Springer (2011)
- [49] Satar, B., Ma, Z., Irawan, P.A., Mulyawan, W.A., Jiang, J., Lim, E.P., Ngo, C.W.: Seeing culture: A benchmark for visual reasoning and grounding (2025), <https://arxiv.org/abs/2509.16517>

- [50] Shafiee, N., Padir, T., Elhamifar, E.: Introvert: Human trajectory prediction via conditional 3d attention. In: 2021 IEEE/CVF Conference on Computer Vision and Pattern Recognition (CVPR). pp. 16810–16820 (2021). doi:[10.1109/CVPR46437.2021.01654](https://doi.org/10.1109/CVPR46437.2021.01654)
- [51] Solera, F., Calderara, S., Cucchiara, R.: Structured learning for detection of social groups in crowd. In: 2013 10th IEEE international conference on advanced video and signal based surveillance. pp. 7–12. IEEE (2013)
- [52] Solera, F., Calderara, S., Cucchiara, R.: Socially constrained structural learning for groups detection in crowd. *IEEE Transactions on Pattern Analysis and Machine Intelligence* **38**(5), 995–1008 (2016). doi:[10.1109/TPAMI.2015.2470658](https://doi.org/10.1109/TPAMI.2015.2470658)
- [53] Su, J., Huang, J., Qing, L., He, X., Chen, H.: A new approach for social group detection based on spatio-temporal interpersonal distance measurement. *Heliyon* **8**(10), e11038 (2022). doi:<https://doi.org/10.1016/j.heliyon.2022.e11038>, <https://www.sciencedirect.com/science/article/pii/S240584402202326X>
- [54] Tan, B.C.Z., Weihua, Z., Liu, Z., Chen, N.F., Lee, H., Choo, K.T.W., Lee, R.K.W.: Blend-vis: Benchmarking multimodal cultural understanding in vision language models (2025), <https://arxiv.org/abs/2510.11178>
- [55] Thompson, S., Gupta, A., Gupta, A.W., Chen, A., Vázquez, M.: Conversational group detection with graph neural networks. In: Proceedings of the 2021 International Conference on Multimodal Interaction. pp. 248–252 (2021)
- [56] Vayani, A., Dissanayake, D., Watawana, H., Ahsan, N., Sasikumar, N., Thawakar, O., Ademtew, H.B., Hmaiti, Y., Kumar, A., Kuckreja, K., Maslych, M., Al Ghallabi, W., Mihaylov, M., Qin, C., Shaker, A.M., Zhang, M., Ihsani, M.K., Esplana, A., Gokani, M., Mirkin, S., Singh, H., Srivastava, A., Hamerlik, E., Asma Izzati, F., Adamsyah Maani, F., Cavada, S., Chim, J., Gupta, R., Manjunath, S., Zhumakhanova, K., Heriniaina Rabevohitra, F., Amirudin, A., Ridzuan, M., Kareem, D., More, K., Li, K., Shakya, P., Saad, M., Ghasemaghaei, A., Djanibekov, A., Azizov, D., Jankovic, B., Bhatia, N., Cabrera, A., Obando-Ceron, J., Otieno, O., Farestam, F., Rabbani, M., Baliyah, S., Sanjeev, S., Shtanchaev, A., Fatima, M., Nguyen, T., Kareem, A., Aremu, T., Xavier, N., Bhatkal, A., Toyin, H., Chadha, A., Cholakkal, H., Anwer, R.M., Felsberg, M., Laaksonen, J., Solorio, T., Choudhury, M., Laptev, I., Shah, M., Khan, S., Khan, F.S.: All languages matter: Evaluating lmms on culturally diverse 100 languages. In: 2025 IEEE/CVF Conference on Computer Vision and Pattern Recognition (CVPR). pp. 19565–19575 (2025). doi:[10.1109/CVPR52734.2025.01822](https://doi.org/10.1109/CVPR52734.2025.01822)
- [57] Veeraraghavan, H., Masoud, O., Papanikolopoulos, N.P.: Computer vision algorithms for intersection monitoring. *IEEE Transactions on Intelligent Transportation Systems* **4**(2), 78–89 (2003)
- [58] Wang, X., Zhang, X., Zhu, Y., Guo, Y., Yuan, X., Xiang, L., Wang, Z., Ding, G., Brady, D., Dai, Q., Fang, L.: Panda: A gigapixel-level human-centric video dataset. In: 2020 IEEE/CVF Conference on Computer Vision and Pattern Recognition (CVPR). pp. 3265–3275 (2020). doi:[10.1109/CVPR42600.2020.00333](https://doi.org/10.1109/CVPR42600.2020.00333)
- [59] Wu, L.F., Wang, Q., Jian, M., Qiao, Y., Zhao, B.X.: A comprehensive review of group activity recognition in videos. *International Journal of Automation and Computing* **18**(3), 334–350 (2021)

- [60] Yokoyama, K., Nakatani, C., Ukita, N.: Dynamic group detection using vlm-augmented temporal groupness graph. In: Proceedings of the IEEE/CVF International Conference on Computer Vision (ICCV). pp. 10475–10484 (October 2025)
- [61] Yu, T., Lim, S.N., Patwardhan, K., Krahnstoeber, N.: Monitoring, recognizing and discovering social networks. In: 2009 IEEE Conference on Computer Vision and Pattern Recognition. pp. 1462–1469. IEEE (2009)
- [62] Zaidenberg, S., Boulay, B., Brémond, F.: A generic framework for video understanding applied to group behavior recognition. In: 2012 IEEE Ninth International Conference on Advanced Video and Signal-Based Surveillance. pp. 136–142. IEEE (2012)
- [63] Zhang, H., Jiang, H., Yao, Q., Sun, Y., Zhang, R., Zhao, H., Li, H., Zhu, H., Yang, Z.: Detect anything 3d in the wild. arXiv preprint arXiv:2504.07958 (2025)
- [64] Zhang, J., Gu, L., Lai, Y.K., Wang, X., Li, K.: Toward grouping in large scenes with occlusion-aware spatio-temporal transformers. IEEE Transactions on Circuits and Systems for Video Technology **34**(5), 3919–3929 (2024). doi:[10.1109/TCSVT.2023.3324868](https://doi.org/10.1109/TCSVT.2023.3324868)

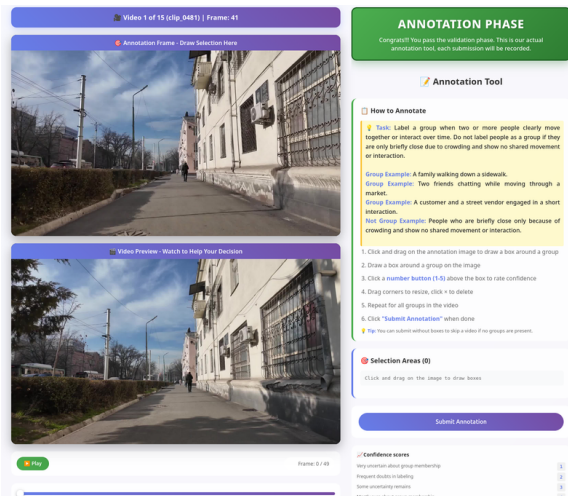
## A. Coarse-grained Annotation Details

Figure 8a illustrates our annotation interface for the coarse-grained annotation task. We ask annotators to create bounding boxes by clicking and dragging on the top canvas. When needed, they can review the corresponding video to verify their decisions. For each bounding box, annotators also assign a confidence score ranging from 1 to 5, following the Likert scale shown in Table 5.

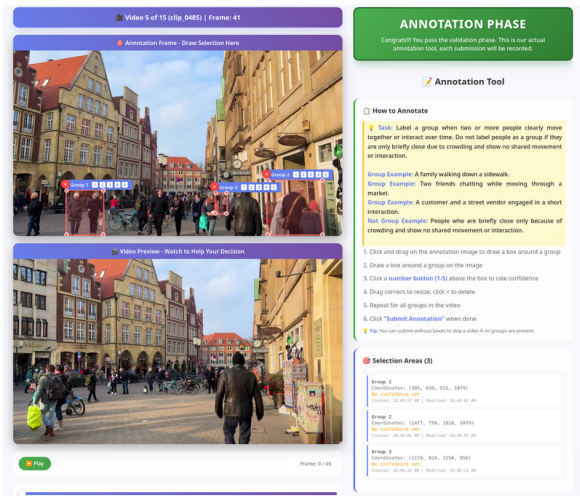
Table 5 | Confidence scale for group membership labeling.

Value	Confidence Level	Description
1	Not confident at all	Very uncertain about group membership
2	Low confidence	Frequent doubts in labeling
3	Moderately confident	Some uncertainty remains
4	Confident	Mostly sure about group membership
5	Very confident	Certain about group detection correctness

After completing a clip, annotators click “Submit annotation” to proceed to the next one, repeating this process until they finish all clips. Each submission creates a database entry that records metadata about the annotation, including the timestamp, the number of actions identified, the video viewing history, and other relevant information. For example, the median annotation time per clip is 30 seconds. In particular, annotators spend a median of 13 seconds on scattered scenes, 38 seconds on moderately populated scenes, and 54 seconds on crowded scenes.



(a) Coarse Annotation interface



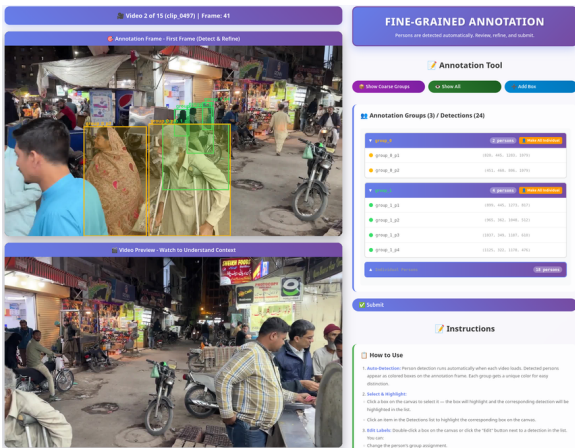
(b) Coarse Annotation interface with boxes

Figure 8 | Coarse annotation tool used for labeling groups.

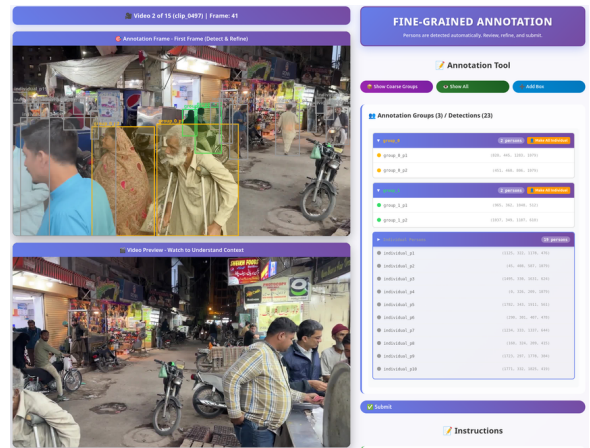
For each frame, we end up with at least 3 annotators. To get a final annotation set, we iterate through each detected group and adding it only if its bounding box does not overlap with any previously included box ( $\text{IoU} \geq 0.3$ ). We adopt this strategy to maximize group detections, as individual annotators may overlook some instances. Figure 10 (left) presents coarse annotations after this procedure.

## B. Fine-grained Annotation Details

Figure 9a illustrates our interface for the fine-grained annotation task. We first propose an initial grouping based on the final set of coarse groups, and then ask annotators to refine these annotations. The initial set of bounding boxes is detected by SAM3 [15] over the full image, as well as over each coarse patch and an additional third of its surrounding area. Annotators can remove bounding boxes, modify the group label assigned to a bounding box, or add new bounding boxes. When necessary, they can review the corresponding video to support their decisions. Figure 9b presents an example after refinement, together with the detected individuals. Similar to the coarse annotation task, clicking the submit button records the annotation in the database and loads the next clip. Figure 10 (right) shows finegrained annotations after this procedure.



(a) Fine-grained Annotation interface before refinement



(b) Fine-grained Annotation interface after refinement

Figure 9 | Fine-grained annotation tool used for labeling groups.

On average, we reach three annotators for each frame, achieving an inter-annotator agreement of 95.56% with the preceding coarse annotations. To consolidate the annotations, we apply a majority-vote scheme combined with a connected-components heuristic. Specifically, each group label must appear in at least half of the annotators' responses, and we match candidate bounding boxes across annotators using an area-adaptive IoU criterion. We retain only connected components with at least two members and merge them to produce the final fine-grained detections, resulting in a fine-grained inter-annotator agreement of 91.64%. Overall, the median annotation time per clip is 22 seconds. For scattered clips, the median time is 6 seconds, for moderately crowded clips 23 seconds, and for crowded clips 53 seconds.

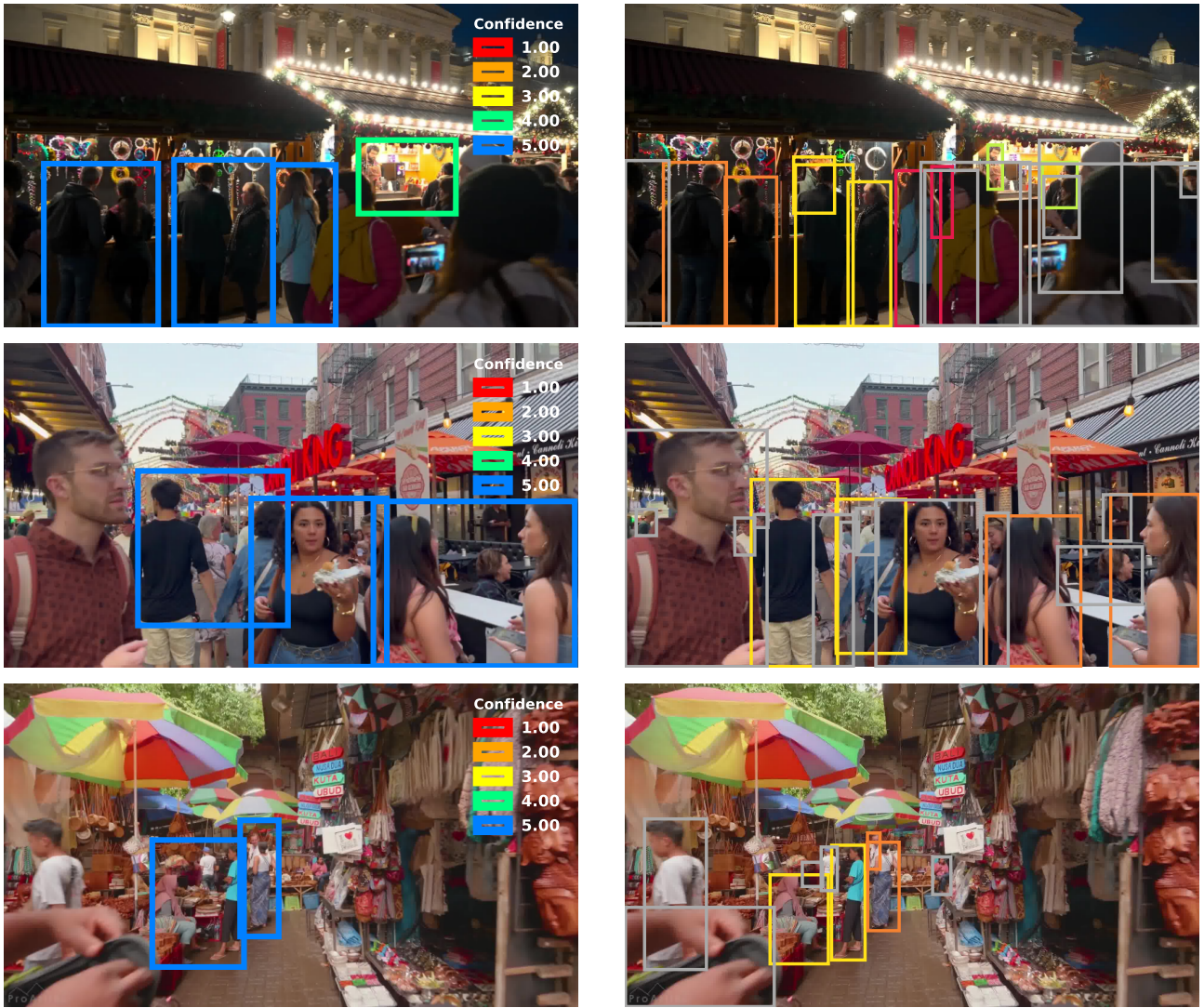


Figure 10 | Examples of coarse (left) and fine-grained (right) annotations.

### C. Analysis of Social Activities

We continue the discussion on analyzing activities across regions, which was then exemplified with Qwen2.5-VL 72B in Figure 6. We now compare across VLMs the counts of activities “walking”, “riding motorcycle”, “moving goods”, and “cooking”. As shown in Figure 11, a consensus among the models indicates a low probability of bias. For example, the appearance of “walking” in all regions and “cooking” or “riding motorcycle” in South-East Asia, respectively, highlights that activities can be region-specific and model agreement can reveal their presence. Conversely, Figure 12 portrays a contrasting scenario with lower agreement. Activities such as “shopping” or “commute” show significant variance between the models. Notably, LLaVA-v1.6 tends to overestimate the frequencies, which could potentially indicate model bias for certain activities.

Given the open-ended nature of our activity recognition experiments, we also present the results of probing for a specific activity. Figure 13 shows the normalized counts of “Hugging” and “Hand-holding”, as a means of understanding proxemics in a region. We obtain these by uniformly sampling clips over countries and regions to ensure fair representation. The counts within samples are normalized by the number of groups and the average of normalized counts across all samples is plotted by region. In the figure, Hand-holding is relatively more common due to its lower-barrier in comparison with Hugging,

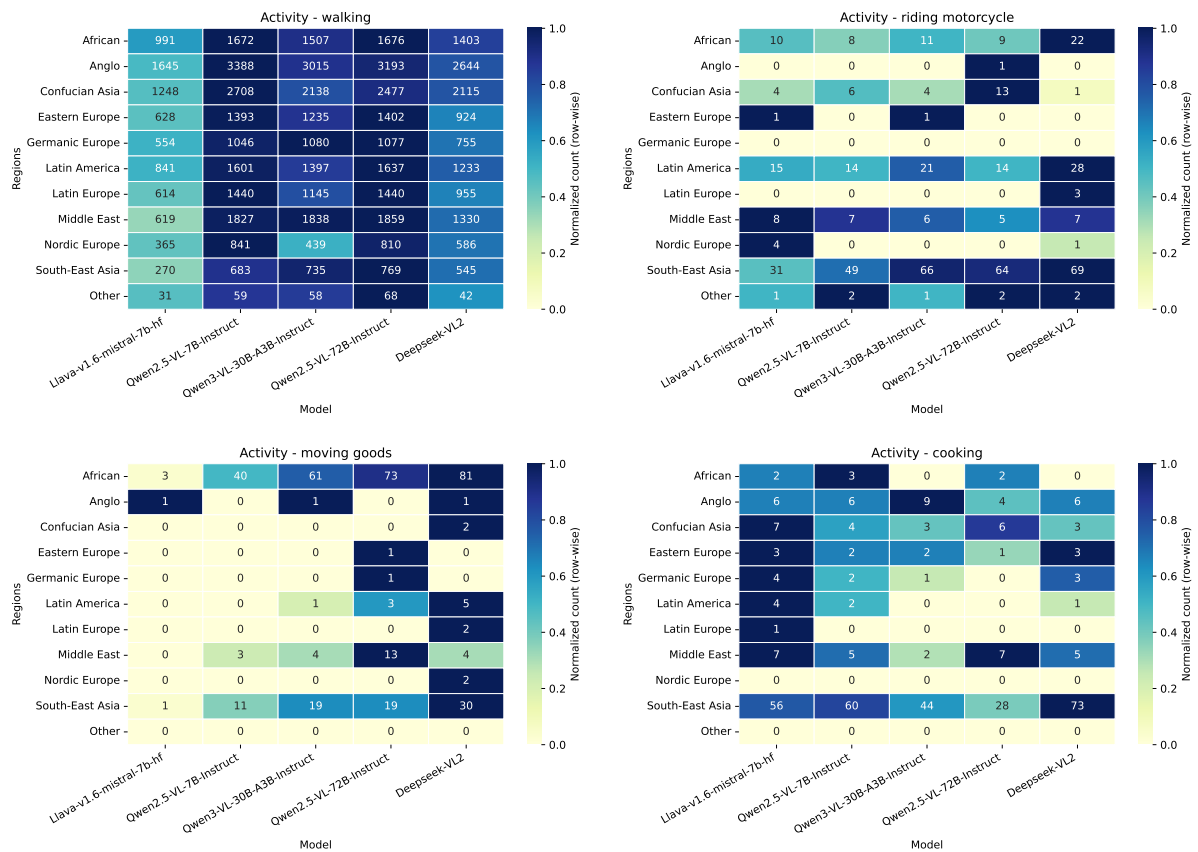


Figure 11 | Regional distribution of activity recognition across VLMs for “riding motorcycle”, “moving goods”, and “cooking”.

which generally requires a higher level of intimacy. Regions such as Eastern Europe or Latin America might reflect genuine behavioral trends; however, the African region may not be truly representative. As before, the models differ in their perceived frequencies, indicating different sensitivities; however, the variations across regions are consistent for all models. For example, African has lower frequencies than Latin America.

In addition, we produce Figure 14 to gain a better perspective of the overall distribution of activities. The plot visualizes embeddings from Qwen3-8B-Embedding by projecting them into a two-dimensional plane with UMAP [41]. Each activity in our fixed, data-driven vocabulary is represented by a circle of radius proportional to its frequency and color coded by its region of occurrence. We observe that, in addition to the differences in the distribution of LLaVA-v1.6, the cluster structures of Qwen2.5-VL 72B and DeepSeek-VL2 are near-identical. Such an analysis is beneficial towards identifying parameter-efficient models that can achieve similar performance as the larger models.

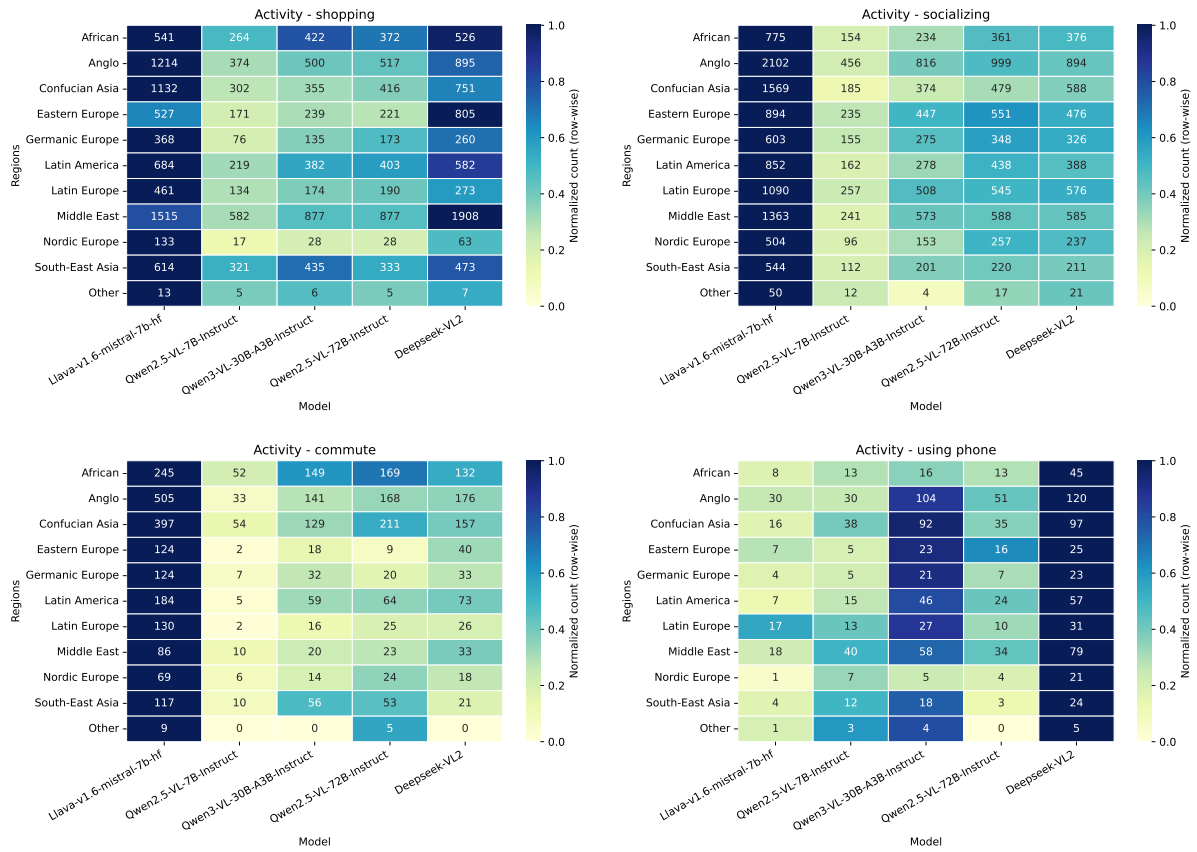


Figure 12 | Regional distribution of activity recognition across VLMs for “commute”, “using phone”, and “socializing”.

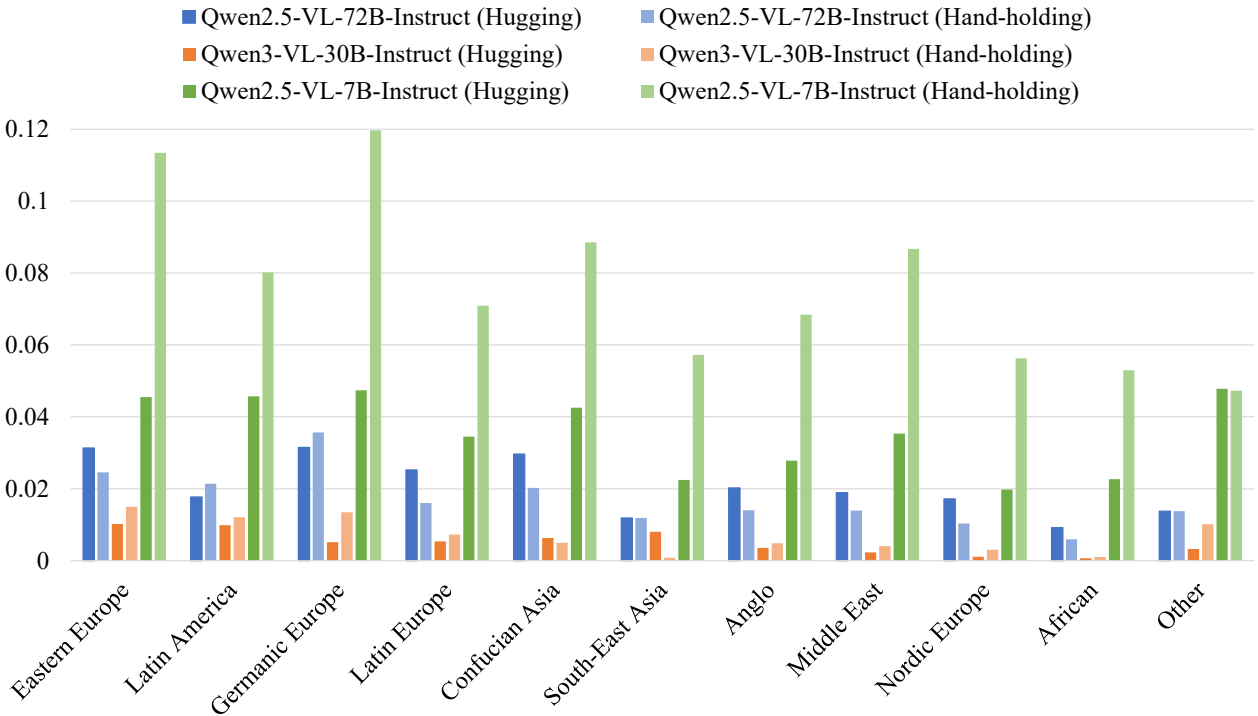
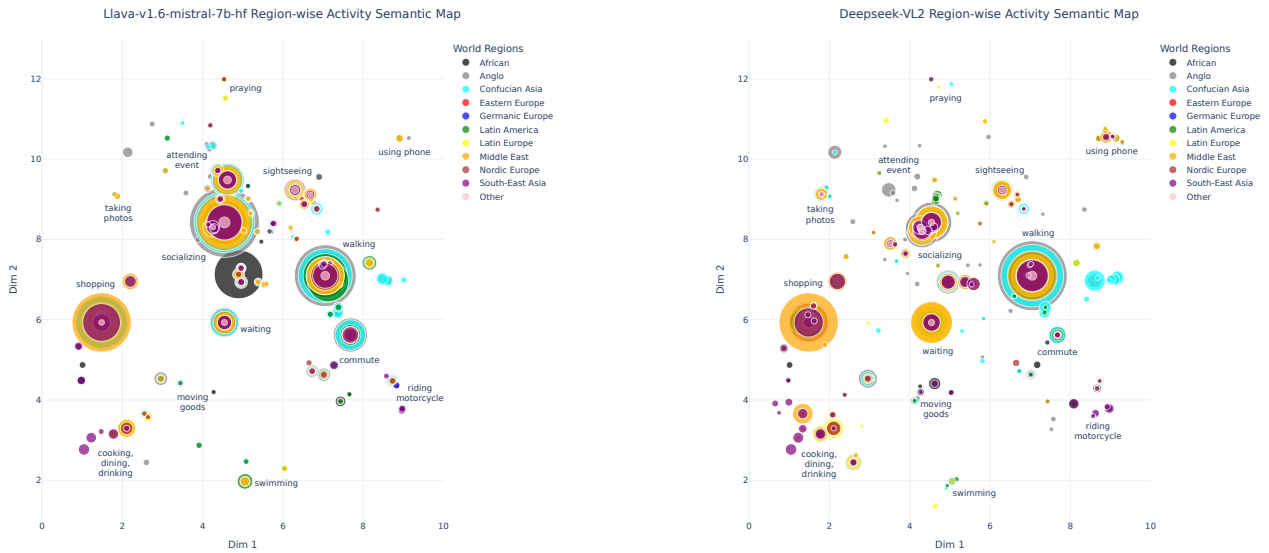
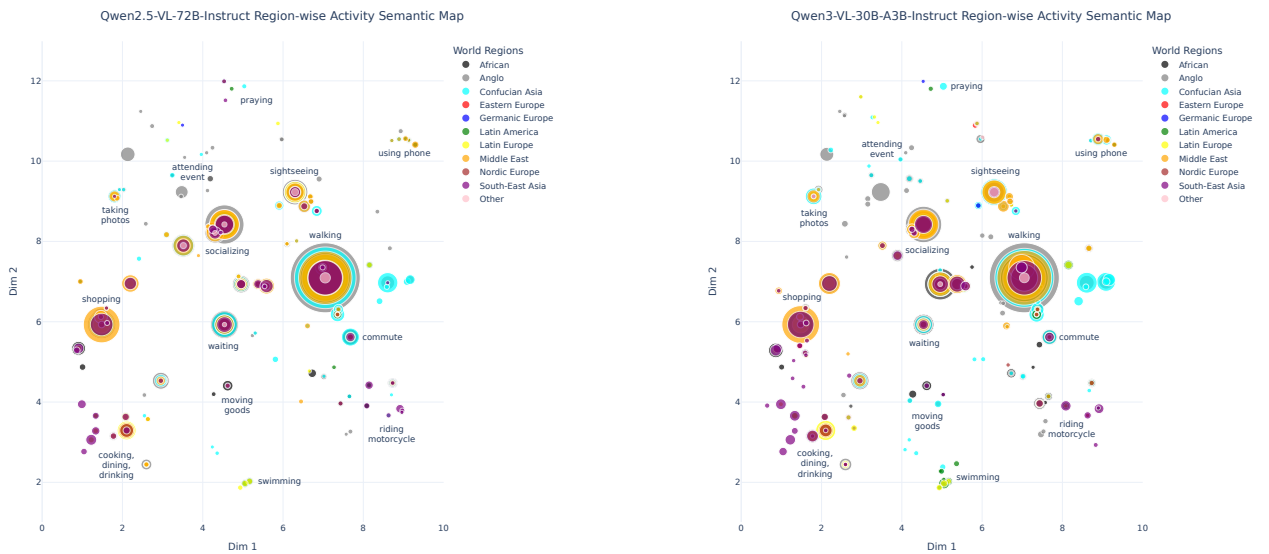


Figure 13 | Distribution of proximity activities (Hugging and Hand holding) grouped by GLOBE regions. Inside a region, each pair lines represent predictions from a different model.



(a) Llava-v1.6

(b) DeepSeek-VL2



(c) Qwen2.5-72B

(d) Qwen3-30B

Figure 14 | Comparison of Semantic Activity Maps across five different models.

## D. Additional Experiments

**EgoGroups.** We also include smaller models in the experiments for *EgoGroups*, such as Cosmos-Reason2 2B, Qwen2.5 (3B–7B), and Qwen3 4B. Table 6 and Table 7 summarizes the results segmented by crowd density using the AP and F1 score, respectively. Notably, Qwen2.5 (3B–7B) outperforms other models in crowded settings (e.g., F1 scores). Table 8 show overall results in terms of F1 and AP metrics. Table 9 reports the AP results segmented by GLOBE region.

**JRDB.** Similarly, Table 10 includes smaller models for the JRDB dataset. In contrast, these smaller models perform worse than larger model variants.

Table 6 | Full fine-grained experiments performance comparison on EgoGroups dataset segmented by crowd density: scattered, moderate and crowded. Model combination indicates the backbone family, number of parameters, and modality. G<sub>1</sub>–G<sub>5</sub> represent AP scores for group sizes 1–5+, where AP is the average performance across groups.

Model		Scattered							Moderate					Crowded						
		G <sub>1</sub>	G <sub>2</sub>	G <sub>3</sub>	G <sub>4</sub>	G <sub>5</sub>	AP	G <sub>1</sub>	G <sub>2</sub>	G <sub>3</sub>	G <sub>4</sub>	G <sub>5</sub>	AP	G <sub>1</sub>	G <sub>2</sub>	G <sub>3</sub>	G <sub>4</sub>	G <sub>5</sub>	AP	
Cosmos-Reason2	2B	VLM	76.21	59.89	61.84	54.86	45.0	59.56	58.4	51.44	55.98	48.75	57.55	54.42	54.69	46.57	49.09	49.07	48.8	49.64
		LLM	71.01	59.22	62.99	60.42	37.12	58.15	55.68	48.81	56.9	62.92	52.45	55.35	48.73	41.51	51.45	52.77	55.81	50.05
	8B	VLM	57.18	74.42	76.36	75.35	80.6	72.78	28.92	45.28	59.54	68.02	68.55	54.06	12.8	30.12	50.05	61.53	73.18	45.53
		LLM	60.72	71.03	72.84	70.49	75.0	70.02	32.47	49.61	65.81	62.54	76.02	57.29	20.58	40.56	55.9	59.69	65.15	48.38
Qwen2.5	3B	VLM	60.06	76.93	71.16	65.63	53.64	65.48	38.75	61.15	68.92	61.92	56.49	57.45	39.46	55.47	62.98	60.16	61.66	55.94
		LLM	75.64	70.24	59.69	59.03	32.88	59.5	57.69	69.58	64.59	53.65	49.75	59.06	48.45	63.46	62.94	51.52	49.29	55.13
	7B	VLM	<b>83.52</b>	68.09	54.34	51.04	45.91	60.58	<b>72.85</b>	65.86	58.96	58.38	49.01	61.01	<b>70.75</b>	61.96	56.23	42.62	45.33	55.38
		LLM	66.25	78.04	79.67	70.48	54.85	69.86	43.94	62.46	70.36	68.22	55.66	60.13	30.2	55.28	70.29	61.53	61.26	55.71
	32B	VLM	58.94	83.37	<b>86.92</b>	<b>81.6</b>	<b>92.27</b>	<b>80.62</b>	30.28	62.72	77.55	<b>84.21</b>	79.38	66.83	19.11	52.42	73.26	76.05	71.56	58.48
		LLM	63.71	85.28	82.38	79.51	62.73	74.72	40.49	73.14	75.28	73.02	70.62	66.51	30.45	64.66	72.69	68.27	64.38	60.09
	72B	VLM	60.53	85.1	85.11	79.17	84.54	78.89	37.18	66.91	<b>79.14</b>	78.45	<b>82.76</b>	<b>68.89</b>	25.89	59.79	<b>73.79</b>	<b>77.81</b>	<b>74.18</b>	<b>62.29</b>
		LLM	63.97	<b>85.84</b>	80.24	75.0	59.55	72.92	38.73	73.68	76.4	71.85	69.28	65.99	28.02	65.93	73.18	68.64	61.92	59.54
Qwen3	4B	VLM	82.16	68.09	70.03	71.88	76.97	73.83	50.47	55.72	61.93	70.38	64.93	60.69	32.31	44.12	58.22	67.86	68.47	54.2
		LLM	68.28	78.47	80.45	72.57	68.94	73.74	46.76	63.03	72.77	77.22	73.2	66.6	35.84	52.57	70.46	70.62	67.86	59.47
	30B	VLM	71.59	80.28	74.26	75.0	59.09	72.04	50.29	66.02	71.33	71.07	70.36	65.81	36.89	57.26	63.7	60.82	58.39	55.41
		LLM	69.41	83.56	79.37	78.47	62.73	74.71	54.94	69.94	71.17	72.14	70.15	67.67	47.59	62.84	69.35	63.25	59.25	60.46
Gemini-3-Pro	VLM	82.67	80.85	73.92	76.39	68.79	76.52	70.37	<b>75.5</b>	68.24	67.24	57.07	67.69	63.09	<b>69.78</b>	64.16	54.43	47.9	59.87	
	LLM	77.66	81.85	75.33	75.35	59.55	73.95	60.29	74.18	73.23	70.9	62.12	68.14	50.95	69.0	68.63	63.71	54.88	61.44	

Table 7 | Full fine-grained experiments performance comparison on EgoGroups dataset segmented by crowd density: scattered, moderate and crowded. Model combination indicates the backbone family, number of parameters, and modality. Precision, Recall, and F1 scores measure the false positive rate of predicted group IDs.

Model		Scattered			Moderate			Crowded			
		Precision	Recall	F1	Precision	Recall	F1	Precision	Recall	F1	
Cosmos-Reason2	2B	VLM	49.03	25.24	33.29	33.97	17.3	22.88	25.88	12.77	17.05
		LLM	38.24	21.5	27.52	32.46	17.74	22.92	26.56	14.07	18.37
	8B	VLM	50.44	49.82	50.1	25.92	16.16	19.9	11.22	5.41	7.3
		LLM	44.73	40.6	42.47	22.04	14.3	17.33	11.75	6.61	8.45
Qwen2.5	3B	VLM	46.41	54.8	50.23	32.77	33.8	33.25	26.81	29.27	<b>27.98</b>
		LLM	41.69	40.13	40.81	34.29	<b>39.04</b>	36.45	23.09	<b>30.58</b>	26.3
	7B	VLM	47.95	34.0	39.66	<b>39.65</b>	32.59	35.66	<b>28.2</b>	26.98	27.57
		LLM	47.76	53.36	50.4	26.32	22.7	24.37	17.23	15.5	16.31
	32B	VLM	51.4	61.87	56.12	27.05	26.18	26.58	14.35	13.69	14.01
		LLM	51.22	64.05	56.88	29.8	33.25	31.41	17.5	21.74	19.38
	72B	VLM	52.77	<b>65.65</b>	58.49	32.76	33.54	33.1	21.0	22.25	21.6
		LLM	51.09	65.36	57.3	28.52	32.39	30.31	15.01	18.98	16.75
Qwen3	4B	VLM	60.6	39.35	47.53	27.85	17.7	21.63	13.93	8.43	10.5
		LLM	53.27	52.36	52.71	29.78	25.1	27.21	13.65	11.77	12.63
	30B	VLM	54.88	56.73	55.7	30.02	25.69	27.68	13.73	12.45	13.06
		LLM	55.96	61.84	58.73	33.72	29.54	31.47	17.92	16.29	17.03
Gemini-3-Pro	VLM	<b>61.02</b>	57.83	<b>59.19</b>	38.44	36.99	<b>37.63</b>	22.75	25.67	24.09	
	LLM	58.0	59.01	58.26	34.59	34.21	34.34	19.28	22.72	20.83	

Table 8 | Full fine-grained experiments performance comparison on the *EgoGroups* dataset. Model combination indicates the backbone family, number of parameters, and input modality. G<sub>1</sub>–G<sub>5</sub> represent AP scores for group sizes 1–5+, with AP showing the average performance across groups. Precision, Recall, and F1 scores measure the false positive rate of predicted group IDs.

Model		G <sub>1</sub>	G <sub>2</sub>	G <sub>3</sub>	G <sub>4</sub>	G <sub>5</sub>	AP	Precision	Recall	F1	
Cosmos-Reason2	2B	VLM	57.49	49.88	52.72	49.29	51.65	52.21	31.37	15.75	20.96
		LLM	52.55	46.24	54.35	57.03	53.26	52.68	30.07	14.01	17.64
	8B	VLM	21.09	40.74	55.68	65.4	72.46	51.07	23.83	14.01	17.64
		LLM	27.27	47.32	60.96	61.9	69.47	53.38	20.59	12.99	15.93
Qwen2.5	3B	VLM	40.9	59.96	65.69	61.21	59.11	57.37	31.16	33.56	32.32
		LLM	53.35	66.57	63.23	52.78	48.08	56.8	28.58	<b>34.78</b>	31.35
	7B	VLM	<b>72.39</b>	64.12	57.06	49.02	46.27	57.77	<b>33.83</b>	29.82	31.69
		LLM	37.12	60.51	71.1	64.68	58.91	58.47	24.34	22.08	23.14
	32B	VLM	25.59	59.72	75.94	<b>79.67</b>	75.91	63.37	23.7	23.32	23.49
		LLM	36.06	70.15	74.43	71.16	66.38	63.64	25.45	30.41	27.7
	72B	VLM	31.96	65.24	<b>76.65</b>	78.27	<b>77.86</b>	<b>66.0</b>	20.09	30.95	29.97
		LLM	34.04	71.03	74.9	70.46	64.22	62.93	23.68	28.78	25.97
Qwen3	4B	VLM	41.65	51.16	60.68	69.21	68.06	58.15	24.29	15.09	18.61
		LLM	41.64	59.39	72.18	73.22	69.79	63.24	24.18	20.97	22.44
	30B	VLM	43.61	63.1	67.4	65.82	62.65	60.51	24.40	21.96	23.11
		LLM	51.49	67.81	70.87	67.8	63.2	64.23	28.34	25.94	27.05
Gemini-3-Pro	VLM	66.8	<b>73.18</b>	66.34	61.16	52.79	64.05	31.76	33.25	<b>32.44</b>	
	LLM	55.82	72.38	70.79	67.47	57.81	64.85	28.24	30.79	29.41	

Table 9 | Full fine-grained experiments performance comparison on the EgoGroups dataset, segmented by GLOBE regions. Model combination indicates the backbone family, number of parameters, and input modality. We report each region’s AP score individually, and compute MAP as the average across all regions. The best and worst values per row are highlighted in red and blue, respectively.

Model		AF	AN	CA	EU	GE	LA	LE	ME	NE	SA	O	
Cosmos-Reason2	2B	VLM	<b>57.13</b>	53.18	53.67	56.16	<b>44.94</b>	47.93	51.12	49.50	46.30	50.67	50.64
		LLM	<b>48.85</b>	51.74	54.61	53.88	51.64	<b>58.28</b>	49.75	50.54	57.31	53.96	53.51
	8B	VLM	47.19	50.49	54.01	51.69	<b>40.07</b>	51.12	52.98	47.05	49.86	52.86	<b>58.89</b>
		LLM	<b>45.95</b>	<b>56.89</b>	55.25	54.59	50.95	54.17	54.40	49.18	51.21	52.95	53.37
Qwen2.5	3B	VLM	55.45	58.24	58.29	58.09	56.34	<b>54.06</b>	55.75	55.14	<b>60.74</b>	56.32	54.53
		LLM	55.86	58.69	55.46	56.71	<b>59.75</b>	57.48	54.51	<b>53.88</b>	57.93	56.55	57.71
	7B	VLM	54.33	58.52	57.26	62.57	61.81	<b>65.47</b>	57.05	<b>50.81</b>	59.05	63.33	56.34
		LLM	55.70	60.27	57.77	<b>52.77</b>	61.74	<b>63.10</b>	59.89	54.37	61.89	60.01	58.42
	32B	VLM	61.99	64.63	63.57	58.82	60.48	66.55	64.09	57.98	<b>71.75</b>	65.75	<b>50.00</b>
		LLM	61.87	65.01	62.16	61.69	62.84	66.89	63.84	<b>59.75</b>	<b>69.36</b>	63.28	61.63
	72B	VLM	<b>58.64</b>	67.24	65.78	64.54	67.06	70.06	67.69	59.42	<b>71.45</b>	67.30	65.80
		LLM	61.94	65.22	61.88	62.32	64.28	65.04	62.61	57.33	<b>67.31</b>	64.49	<b>54.21</b>
Qwen3	4B	VLM	60.17	58.78	60.25	59.91	61.57	<b>53.04</b>	56.21	56.47	53.61	53.53	<b>61.83</b>
		LLM	58.31	65.44	62.48	64.49	60.82	<b>69.47</b>	65.44	57.79	65.56	62.83	<b>52.35</b>
	30B	VLM	56.07	64.76	58.49	60.26	<b>65.85</b>	59.92	63.42	<b>53.94</b>	56.30	64.20	63.10
		LLM	62.64	65.61	64.43	65.95	66.34	66.73	63.30	57.70	<b>67.66</b>	66.31	<b>55.60</b>
Gemini-3-Pro	VLM	62.41	66.70	64.01	68.23	65.53	64.79	64.32	<b>60.24</b>	<b>71.84</b>	66.03	62.31	
	LLM	60.87	64.59	64.69	<b>68.61</b>	64.37	62.55	66.47	<b>59.51</b>	62.44	66.69	64.70	

Table 10 | Fine-grained performance comparison on the JRDB dataset. Model combination indicates the backbone family, number of parameters, and input modality.  $G_1$ – $G_5$  represent AP scores for group sizes 1–5+, with AP showing the average performance across all groups. Precision, Recall, and F1 scores measure the false positive rate of predicted group IDs.

Model		Group Detection (AP)					Group ID Prediction				
		$G_1$	$G_2$	$G_3$	$G_4$	$G_5$	AP	Precision	Recall	F1	
JLSG [19]		8.0	29.30	37.5	65.40	67.0	41.4	-	-	-	
JRDB-Act [20]		81.40	64.80	49.10	63.20	37.20	59.2	-	-	-	
DVT3 [60]		-	-	-	-	-	-	<b>61.16</b>	31.06	41.19	
Cosmos-Reason2	2B	VLM	75.59	45.6	33.17	32.3	28.3	42.99	16.41	2.33	4.09
		LLM	51.93	39.46	36.07	36.91	42.05	41.28	17.06	3.49	5.79
	8B	VLM	44.88	34.7	30.96	36.83	55.0	40.47	19.83	5.83	9.02
		LLM	48.47	36.19	29.05	31.71	56.26	40.34	24.7	6.93	10.82
Qwen2.5	3B	VLM	65.99	51.13	42.73	37.84	30.3	45.6	12.46	4.82	6.96
		LLM	55.79	45.63	36.24	35.15	47.36	44.03	11.87	4.07	6.07
	7B	VLM	<b>79.02</b>	50.55	38.56	32.05	24.07	44.89	12.54	7.28	9.21
		LLM	33.58	40.37	36.47	39.93	69.4	43.95	12.56	4.92	7.07
	32B	VLM	25.54	47.44	47.23	54.03	69.3	48.71	22.39	16.81	19.2
		LLM	35.13	56.78	54.11	56.96	69.49	54.49	28.45	23.88	25.97
	72B	VLM	28.4	45.44	43.62	51.26	71.99	48.14	23.54	17.28	19.93
		LLM	32.95	55.42	55.34	60.99	66.86	54.31	28.98	25.46	27.11
Qwen3	4B	VLM	48.95	38.65	32.13	34.48	57.97	42.44	16.64	4.56	7.16
		LLM	39.54	44.46	43.99	56.21	64.12	49.66	23.58	11.09	15.08
	30B	VLM	30.5	44.2	41.5	44.71	72.48	46.68	30.19	17.45	22.12
		LLM	47.15	57.38	54.45	57.97	66.62	56.71	40.25	27.84	32.91
	235B	VLM	31.54	44.28	41.36	50.59	77.24	49.0	36.80	21.51	27.15
		LLM	31.0	51.29	60.4	69.63	<b>79.95</b>	58.46	34.03	25.53	29.17
Gemini-3-Pro	VLM	56.66	<b>71.79</b>	79.33	79.7	57.49	68.99	42.99	<b>46.38</b>	<b>44.62</b>	
	LLM	51.65	69.97	<b>82.52</b>	<b>81.8</b>	64.08	<b>70.0</b>	40.89	43.97	42.37	

## E. More Qualitative Examples

Figure 15 shows additional qualitative results of our approach across frames with varying crowd densities (scattered, moderate, and crowded) and different models (Nvidia-Cosmos2 8B, Qwen2.5-72B, Qwen3-30B, Gemini-3-Pro) along with the groundtruth (top) for our *EgoGroups*. Detections with the same color are judged to be in the same social group. We observe that model variants with fewer parameters often struggle to detect reasonable grouping in moderate and crowded scenarios.

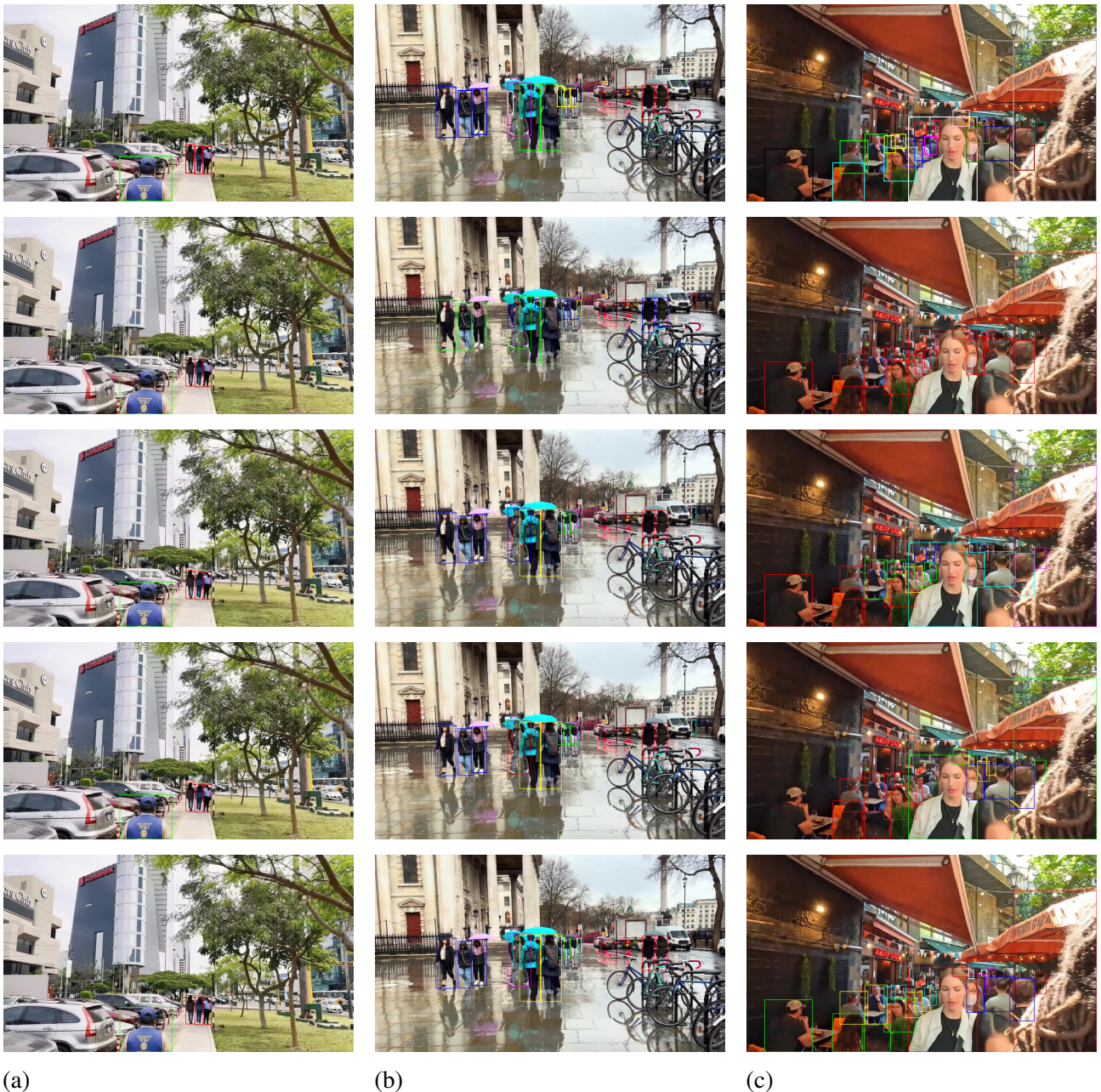


Figure 15 | Qualitative results across frames with varying crowd densities. From left to right: (a) scattered, (b) moderate, and (c) crowded. From top to bottom: ground truth, Nvidia-Cosmos2 8B, Qwen2.5 72B, Qwen3 30B, and Gemini-3-Pro. Detections with the same color are judged to be in a social group.

## F. Prompt Details

Finally, Figures 16, 17, and 18 provide detailed text descriptions of the prompts for LLMs and VLMs, following our inference code, structured using the DSPy framework.

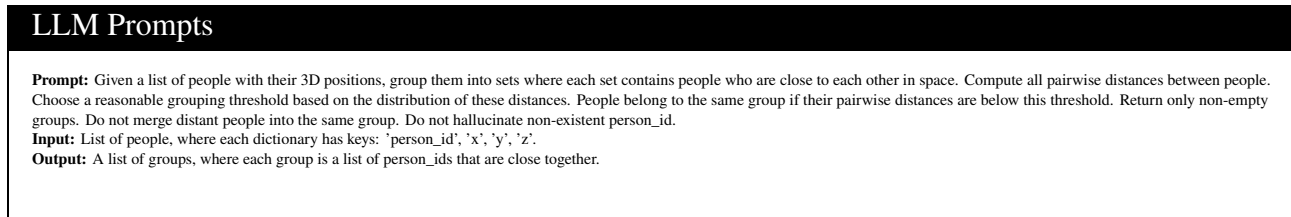


Figure 16 | Prompt instruction and input/output field descriptions processed by LLM.

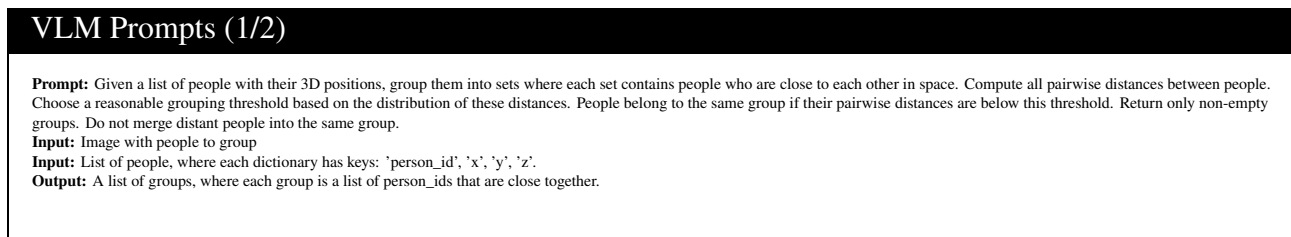


Figure 17 | Prompt instruction and input/output field descriptions processed by VLMs.

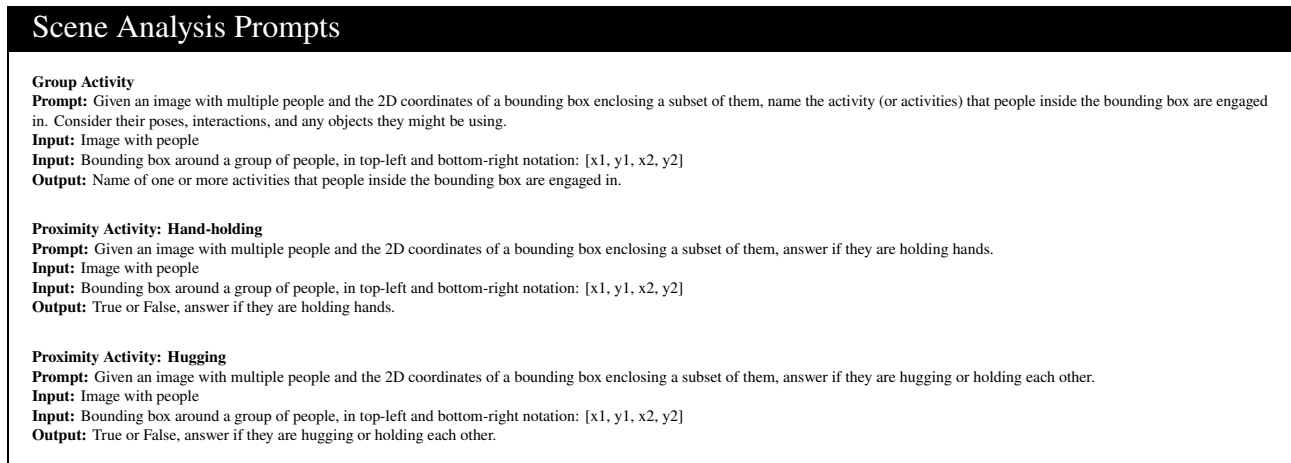


Figure 18 | Prompt instruction and input/output field descriptions processed by VLM for the results in Figure 13.